

DECLASSIFIED: US 1391
DROBKA TO LEEBOW MEMO
DATED 6/30/66

NACA

SERVICE REPORT

Declassified by authority of NASA
Classification Change Notices No. 70
Dated ** 4/20/66

RESEARCH MEMORANDUM

for the

Bureau of Aeronautics, Department of the Navy

TRANSONIC WIND-TUNNEL INVESTIGATION
OF STATIC LONGITUDINAL STABILITY AND CONTROL
CHARACTERISTICS AND DRAG OF A 0.05-SCALE MODEL
OF THE CHANCE VOUGHT XF8U-3 AIRPLANE

TED NO. NACA AD 3133

By P. Kenneth Pierpont

Langley Aeronautical Laboratory
Langley Field, Va.

NATIONAL ADVISORY COMMITTEE
FOR AERONAUTICS

WASHINGTON

SEP 20 1957

CONFIDENTIAL

CONFIDENTIAL
NATIONAL ADVISORY COMMITTEE FOR AERONAUTICS

RESEARCH MEMORANDUM

for the

Bureau of Aeronautics, Department of the Navy


TRANSONIC WIND-TUNNEL INVESTIGATION
OF STATIC LONGITUDINAL STABILITY AND CONTROL
CHARACTERISTICS AND DRAG OF A 0.05-SCALE MODEL
OF THE CHANCE VOUGHT XF8U-3 AIRPLANE

TED NO. NACA AD 3133

By P. Kenneth Pierpont

SUMMARY

A transonic wind-tunnel investigation was made in the Langley 8-foot transonic pressure tunnel at the request of the Bureau of Aeronautics, Department of the Navy, of the static longitudinal stability and control characteristics and drag of a 0.05-scale model of the Chance Vought XF8U-3 airplane at Mach numbers from 0.80 to 1.20 with an average Reynolds number of 2.6×10^6 . The investigation included effects of the addition of the ventral fins, extension and removal of the missiles, deflection of the speed brake, addition of a fuselage fairing near the wing leading edge, and longitudinal control effectiveness. The model was statically stable throughout most of the range of positive lift coefficients, but some loss in horizontal-tail effectiveness may be expected near zero lift and a Mach number of 1.0. Installation of the ventral fins increased the longitudinal stability from 2 to 4 percent at a small drag-coefficient penalty. The speed-brake drag increment decreased with increasing angle of attack, and trim changes of about 2° at low angles of attack may be expected at supersonic speeds. The increase in subsonic drag coefficient caused by extension of the three missiles to firing position was more than three times as great as the increase in drag-coefficient rise at supersonic speeds.



CONFIDENTIAL

INTRODUCTION

The Chance Vought XF8U-3 airplane is an all-weather missile-carrying fighter airplane derived essentially by scaling up a fully area-ruled version of the Chance Vought XF8U-1 airplane, model tests of which are reported in references 1 and 2. The present airplane incorporates thinner wing and tail surfaces which, together with a substantially larger fuselage than the XF8U-1, result in both fineness ratio and area distributions which are essentially the same as those of the XF8U-1 with full area-rule treatment. Tests at transonic and supersonic speeds to evaluate the longitudinal and lateral stability characteristics of a 0.05-scale model of the XF8U-3 airplane were requested by the Bureau of Aeronautics, Department of the Navy. The present paper presents results of a transonic-speed investigation in the Langley 8-foot transonic pressure tunnel of the static longitudinal stability and control characteristics and drag. The investigation included effects of the addition of the ventral fins, extension and removal of the missiles, deflection of the speed brake, addition of a fuselage fairing near the wing leading edge, and longitudinal control effectiveness. Some comparisons are made with data of the XF8U-1 airplane and with unpublished supersonic data obtained in the Langley Unitary Plan wind tunnel.

The Mach numbers extended from 0.80 to 1.2 and the angles of attack from about -10° to 16° . Most of the data were obtained at a total pressure of 1 atmosphere which corresponds to an average Reynolds number of about 2.6×10^6 ; however, because of the balance load limitations, some data were obtained at a total pressure of $1/2$ atmosphere or a Reynolds number of about 1.3×10^6 .

NOTATIONS AND SYMBOLS

All the data, measured with respect to body axes, have been reduced to standard coefficient form with moments and forces referred to the stability-axes system (fig. 1). The pitching-moment reference was at 25 percent mean aerodynamic chord.

C_L lift coefficient, $\frac{\text{Lift}}{qS}$

C_D drag coefficient, $\frac{\text{Drag}}{qS}$


C_m pitching-moment coefficient, $\frac{\text{Pitching moment}}{qS\bar{c}}$

DECLASSIFIED

A	cross-sectional area normal to longitudinal axis
b	wing span
c	chord of wing parallel to free stream
\bar{c}	mean aerodynamic chord of wing, determined without chord-extensions
l	model overall length
L/D	lift-drag ratio
M	Mach number
q	dynamic pressure
S	wing area
R	Reynolds number based on wing mean aerodynamic chord
x	distance rearward, measured either from model nose or reference origin
α	angle of attack of fuselage reference line
i_t	incidence of horizontal tail relative to fuselage reference line in plane of symmetry
C_{mC_L}	rate of change of C_m with respect to C_L
$C_{L\alpha}$	rate of change of C_L with respect to α
C_{mi_t}	rate of change of C_m with respect to i_t
ΔC_D	increment of drag coefficient
ΔC_m	increment of pitching-moment coefficient

Subscripts:

min	minimum
max	maximum



CONFIDENTIAL

d speed brakes
t tails
o zero lift


Model designations:

B fuselage
C missile cavities faired smooth
D speed brake
G fuselage fairing
H horizontal tail
R rocket-motor fairing
S Sparrow missiles
S^E Sparrow missiles extended 1 inch normal to fuselage surface
to simulate firing position
V₁ vertical tail
V₂ ventral fins
W wings

MODELS AND APPARATUS

Models

The model used for this investigation was a 0.05-scale model of the Chance Vought XF8U-3 airplane. An illustration of the model mounted in the Langley 8-foot transonic pressure tunnel is given in figure 2, and three-view drawings of it are given in figure 3. Area distributions normal to the model axis are presented in figure 4. The model was tested with no internal flow but instead had a faired nose. The wing employed was tested at -1° incidence and had leading-edge chord-extensions. The quarter-chord sweepback was 42° , the aspect ratio was 3.47, and the taper ratio was 0.23. The wing incorporated no camber or twist and utilized an NACA 65A005 root section and NACA 65A004 tip section. The tail surfaces



CONFIDENTIAL

and ventral fins were swept back 45° at the quarter-chord line and employed NACA 65A004 airfoil sections.

Longitudinal control was obtained with an allmovable horizontal tail with the axis of rotation normal to the plane of symmetry. Three Raytheon Sparrow 3 missiles were located in a semisubmerged position on the bottom of the fuselage ahead of the center of gravity. Interchangeable parts permitted extension of the missiles to simulate the firing position. A single speed brake was located on the bottom of the fuselage near the center of gravity; and an auxiliary rocket-motor fairing was installed for one test at the base of the vertical fin. Details of the model are given in table I, and photographs of several of the test configurations are shown in figure 5. One additional configuration consisted of the addition of a large fairing on the fuselage extending rearward from the windshield and beyond the wing leading edge. (See figs. 3 and 5(c).)


Instrumentation

The forces and moments were measured by an internally mounted six-component strain-gage balance. The model angle of attack was obtained by correcting sting-measured angles for the effects of aerodynamic loads. All force, pressure, and angle-of-attack data were recorded electronically by means of a punched-card system.

TESTS

The investigation was conducted in the Langley 8-foot transonic pressure tunnel described in reference 1. The static-longitudinal-stability data were obtained at constant Mach numbers from 0.8 to 1.2 and an angle of sideslip of 0° through an angle-of-attack range from about -10° to 16° , the upper end of the range being limited by balance loads. Some data were obtained at a total pressure of $1/2$ atmosphere in order to extend the range of angles of attack available within the balance limitations. A summary of the configurations and tests reported herein is presented in table II. The average test Reynolds number plotted as a function of Mach number is shown in figure 6.

Most of the data were obtained with the model clean and smooth; however, some of the effects of fixing transition were obtained. Transition was fixed with a $1/8$ -inch-wide band of carborundum of 0.0049-inch average size and with a grain density estimated to average 30 grains per lineal inch. These bands were attached to the body 4 inches from the nose and on the wing upper and lower surfaces at the 10-percent-chord station. Similar bands of lacquer $1/8$ -inch wide, but without carborundum, were



CONFIDENTIAL

applied at the 10-percent-chord station for all tail surfaces, including the ventral fins.

REDUCTION OF DATA

The force along the longitudinal body axis, measured by the strain gage, was adjusted so that the result corresponded to that for a pressure at the model base equal to free-stream static pressure. When the rocket-motor fairing was installed, the base area was considered to be the sum of the model base and rocket-motor-fairing base. No sting-interference corrections have been made apart from the base-pressure adjustment described. Buoyancy corrections were estimated and considered negligible.

Wind-tunnel wall-interference effects at subsonic speeds for the 8-foot transonic pressure tunnel were within the accuracy of the data according to references 3 and 4. At supersonic speeds, between $M = 1.03$ and about 1.18, effects of wall-reflected disturbances were large; no data are, therefore, presented in this range. At other supersonic speeds, effects of wall-reflected disturbances were considered negligible. No corrections for wind-tunnel wall interference have, therefore, been applied to any of the data.

The accuracy of the data from these tests estimated largely on the basis of repeatability of the results are estimated to be as follows:

α , deg	± 0.1
M	± 0.005
C_L	± 0.01
C_D	± 0.001
C_m	0.004

RESULTS AND DISCUSSION

The results are presented in the form of basic longitudinal-stability curves and summary-data curves. Basic longitudinal-stability data (figs. 7 to 12) are given as functions of lift coefficient, whereas most of the summary data (figs. 13 to 22) are prepared as functions of Mach number. A comparison of data at transonic speeds with unpublished supersonic-speed data obtained in the Langley Unitary Plan wind tunnel are given in figure 23. An index of the basic and summary data is provided by table II.

Static Longitudinal Stability and Control


The model with an assumed center-of-gravity location at $0.25\bar{c}$ is shown in figure 7 to have been longitudinally stable through most of the test range of lift coefficients for either the wing body alone or the complete model. At $M = 0.925$ with the highest test lift coefficient, a pitch-up is indicated for the wing-body combination; however, after the installation of the tail surfaces, no unstable tendency seems to remain. This pitch-up is similar to that indicated in reference 1 for the Chance Vought XF8U-1 airplane. At negative lift coefficients greater than 0.5, the data show unstable trends with or without tails for Mach numbers between 0.90 and 0.95. Apparently, the horizontal tail (which was located beneath the wing chord plane) had, at these large negative angles of attack, entered the wing wake and hence became ineffective.

Effects on the stability over the lift-coefficient range for these tests which resulted from the various model modifications are given by figures 7 to 12. Principal results of the configuration changes were in the form of overall slope changes C_{mC_L} which have been plotted for

$C_L = 0$ in figure 13. From this figure none of the modifications caused significant changes in longitudinal stability at subcritical speeds. Addition of the ventral fins increased the stability from 2 to 4 percent at supercritical speeds. Fixing transition is shown to have reduced the stability about 2 percent over the entire Mach number range. Removal of the three missiles increased the stability as much as 5 percent, whereas extending them to firing position caused a decrease of about the same magnitude.

Variation of the pitching-moment contribution of the tails is shown in figure 14 where $\Delta C_{m,t}$ is plotted as a function of Mach number. Relatively small fluctuations in tail pitching-moment increment with Mach number occurred near $\alpha = 0^\circ$; whereas a large increase is shown for $\alpha = 8^\circ$. This increase occurred at the drag-rise Mach number and amounted to $\Delta C_{m,t} = -0.037$. If changes in dynamic pressure at the tail plane are neglected, this increment amounts to a change in tail lift coefficient of nearly 0.2 for $0.92 < M < 0.98$.

Horizontal-tail-effectiveness parameter $C_{m_{it}}$ was obtained from an angle of incidence of 10° and is shown in figure 15. The shape of the curve is approximately the same as that reported in reference 1. The present model, however, exhibits slightly greater horizontal-tail effectiveness than did the XF8U-1. This improvement may have resulted from the fact that the present model stabilizer incorporated no dihedral, whereas that of reference 1 had about 5° dihedral. At negative angles of attack figure 15 shows that the tail effectiveness decreased a small amount.



CONFIDENTIAL

The principal effect on the longitudinal-stability characteristics of deflecting the speed brake 60° is shown by figures 10(c) and 16 to be in the form of trim changes at transonic speeds. Stabilizer deflections somewhat more than 2° are required to trim the airplane at supersonic speeds upon speed-brake deflection; then, as the aircraft decelerates to subcritical speeds, further stabilizer changes up to about 3° may be expected. Increasing the angle of attack will decrease both the initial trim change as well as the change with Mach number.


Representative curves of lift-curve slope have been included and are given in figure 17. The configurations were selected to show the effect of installation of the tails and then the ventral fins. The curves are conventional in both shape and magnitude except that, in comparison with the data of reference 1, the use of the thinner wing has resulted in about a 10-percent decrease in lift-curve slope.

Drag

Comparison of the minimum drag-coefficient levels for most of the configurations is afforded by figure 18. Installation of the tails resulted in a subcritical drag-coefficient increase of about 0.0035 or 35 drag counts with a further increase of about 20 counts at supersonic speeds. Ventral fins contributed no measurable change subsonically and about 20 counts supersonically; however, when the rocket-motor fairing was installed, a supercritical decrease of about 10 counts was observed.

Fixing transition on the complete model is shown by figure 18 to have resulted in a nearly uniform increase in drag coefficient of about 25 counts. Removing the three missiles provided a decrease in drag coefficient through the entire Mach number range of about 0.0015, and filling in the remaining cavities smooth with the fuselage surface reduced the drag-coefficient rise by 10 counts. (See fig. 19.) When the missiles were all extended by means of struts an average distance normal to the fuselage surface of about 1 inch, the subsonic drag-coefficient level increased nearly 75 counts and the drag-coefficient rise increased as much as 20 counts. For the complete model, if a subsonic drag-coefficient level of about 0.015 was assumed, the transonic drag rise amounted to about 150 percent.

Comparison of the present XF8U-3 model with the XF8U-1 of reference 1 shows that the present model incorporated thinner wings and empennage than the XF8U-1; the fuselage, however, was considerably enlarged to allow for an increase in powerplant and armament. An examination of the area distributions for the two models, then, indicates generally good agreement both as to shape as well as magnitude. Therefore, comparison of the XF8U-3 drag results with those of reference 1 (fuselage 3 or 4) indicates the generally expected good agreement.



CONFIDENTIAL

Recent unpublished test results obtained in the 8-foot transonic pressure tunnel, for a symmetrically mounted wing on a symmetrical body to which had been added a fairing on the top of the fuselage in the vicinity of the wing leading edge, indicated that the drag coefficient at low lift coefficients could be reduced, thereby increasing the lift-drag ratio for cruise lift coefficients. By applying the same design principles to the present high-wing configuration, a fairing designed for $M = 1.4$ was installed on the top of the fuselage as shown in figure 5(c). The anticipated drag reduction at lifting conditions did not materialize (fig. 9); nevertheless, no significant minimum-drag change occurred either. (See also fig. 18.) Inasmuch as the added fairing apparently caused no adverse effects, it is suggested that the added volume may prove useful as space for an additional crew member.

The increment in drag coefficient resulting from a 60° speed-brake deflection is shown in figure 20. In general, $\Delta C_{D,d}$ from 0.03 to 0.05 may be expected to be available for deceleration. A general increase in drag increment with Mach number is shown, and unpublished data from the Langley Unitary Plan wind tunnel show that the speed-brake increment varies little with further Mach number increases. Figure 20 also shows a generally decreasing drag-coefficient increment with increasing angle of attack.

Performance


The untrimmed variation of lift-drag ratio as a function of lift coefficient is shown in figure 21 to illustrate the effects of the addition of tails to the wing-body combination. For the purpose of

examining the range performance of the airplane, the function $\frac{C_L^{1/2}}{C_D}$

has been calculated for trimmed conditions at several altitudes and is plotted in figure 22. This function is more useful for turbojet-powered airplanes than the frequently used L/D function. From the data presented, flight at 35,000 feet up to $M = 1.2$ will provide the maximum range performance. For somewhat higher speeds it appears that flying at an altitude of 50,000 feet may provide improved range capability. These data were calculated for combat wing loadings.

Comparison of Transonic and Supersonic Tests

Results from the present tests at transonic speeds in the Langley 8-foot transonic pressure tunnel have been combined with unpublished data obtained at supersonic speeds of $M = 1.6, 1.9,$ and 2.2 in the Langley Unitary Plan wind tunnel in figure 23. The three parameters - lift-curve




CONFIDENTIAL

slope, static-longitudinal-stability parameter, and zero-lift drag coefficient - are shown faired through the transonic to supersonic speed range. Wing-body-alone and complete-model data are shown.

An additional comparison has been made in figure 23 of the zero-lift drag coefficients to include data obtained from tests of various versions of the XF8U-1 in both wind tunnel (ref. 1) and free flight by rocket-boasted models (ref. 2). Two configurations are shown, one in which only partial area ruling was incorporated in the form of a lengthened forebody and afterbody, and the other on which fuselage additions or bumps were applied to smooth the remaining area deficiencies. The data for the latter configuration are shown to agree closely with the model data of the present tests for Mach numbers less than about 1.4. The design Mach number for the former model was 1.2, whereas the present model was designed for a Mach number of 1.4.

SUMMARY OF RESULTS

Wind-tunnel tests have been made in the Langley 8-foot transonic pressure tunnel of the static longitudinal stability and control characteristics and drag of a 0.05-scale model of the Chance Vought XF8U-3 airplane at Mach numbers from 0.80 to 1.2. Reynolds numbers for most of the tests were about 2.6×10^6 . The principal results are summarized as follows:

1. The model was statically stable longitudinally throughout most of the test range of positive lift coefficients. Mild instability was indicated at negative lift coefficients greater than 0.5 between Mach numbers from 0.90 to 0.95.
 2. Stabilizer effectiveness was generally uniform throughout the lift-coefficient and Mach number range except for some loss near zero lift and a Mach number of 1.0.
 3. Installation of the ventral fins added about 0.0020 to the drag-coefficient rise and increased the longitudinal stability from 2 to 4 percent.
 4. The speed-brake drag increment decreased with increasing angle of attack. Trim changes of about 2° may be expected at supersonic speeds; these trim changes decreased with increasing angle of attack.
- 

CONFIDENTIAL

5. Extension of the missiles to simulated firing position increased the level of subsonic drag coefficient by about 0.0075 and the drag-coefficient rise by about 0.0020.

Langley Aeronautical Laboratory,
National Advisory Committee for Aeronautics,
Langley Field, Va., August 26, 1957.

P. Kenneth Pierpont
P. Kenneth Pierpont

Approved:

Eugene C. Draley
Eugene C. Draley

Aeronautical Research Engineer

Chief of Full-Scale Research Division

sam

REFERENCES

1. Pierpont, P. Kenneth: Transonic Wind-Tunnel Investigation of Static Longitudinal and Lateral Stability and Control Characteristics and Drag Rise of a 0.042-Scale Model of the Chance Vought XF8U-1 Airplane - TED No. NACA DE 392. NACA RM SL56I19, Bur. Aero., 1956.
2. Hastings, Earl C., Jr.: Minimum Drag of Four Versions of a Swept-Wing Fighter Airplane Obtained From Flight Tests of Rocket-Boosted Models at Mach Numbers From 0.81 to 1.71. NACA RM L56E25a, 1956.
3. Whitcomb, Charles F., and Osborne, Robert S.: An Experimental Investigation of Boundary Interference on Force and Moment Characteristics of Lifting Models in the Langley 16- and 8-Foot Transonic Tunnels. NACA RM L52L29, 1953.
4. Davis, Don D., Jr., and Moore, Dewey: Analytical Study of Blockage- and Lift-Interference Corrections for Slotted Tunnels Obtained by the Substitution of an Equivalent Homogeneous Boundary for the Discrete Slots. NACA RM L53E07b, 1953.

CONFIDENTIAL

TABLE I.- MODEL DIMENSIONS

[All dimensions are in inches]

Complete model:		
Overall length		36.725
Frontal area		17.90
Fineness ratio		7.69
Frontal area to wing area		0.110
Center-of-gravity location, percent \bar{x}		0.25
Center-of-gravity location, fuselage station		22.55
Wing (W):		
Root airfoil section	NACA 65A005	
Tip airfoil section	NACA 65A004	
Root chord		11.02
Tip chord, extended		2.80
Tip chord, basic		2.50
Span, projected		24.07
Area, projected (excluding extensions)		162.0
Area, projected (including extensions)		167.0
Aspect ratio		3.47
Taper ratio		0.23
Mean aerodynamic chord		7.67
Spanwise location		4.74
Longitudinal location, fuselage station		20.06
Sweepback, leading edge, deg		47.1
Sweepback, $c/4$, deg		42.0
Dihedral, deg		-5.0
Incidence at root chord, deg		-1.0
Twist, deg		0
Location of root chord, above reference axis		1.39
Location of root chord, longitudinal		15.54
Horizontal tail (H):		
Root airfoil section	NACA 65A004	
Tip airfoil section	NACA 65A004	
Root chord		6.36
Tip chord		0.95
Span, projected		12.80
Total area, projected		46.8
Exposed area, projected		27.90
Aspect ratio, based on total area		3.50
Taper ratio		0.15
Dihedral, deg		0
Sweepback, $c/4$, deg		45
Location of root chord, longitudinal		29.15
Location of root chord, above or below reference axis		-0.26
Location of axis of rotation, longitudinal		33.91
Vertical tail (V_1):		
Root airfoil section	NACA 65A004	
Tip airfoil section	NACA 65A003	
Root chord		5.61
Tip chord		2.28
Span, total		7.25
Span, exposed		5.60
Area, exposed		22.07
Aspect ratio, based on exposed area		1.42
Taper ratio		0.41
Sweepback, leading edge, deg		50
Sweepback, $c/4$, deg		45
Location of root chord, longitudinal		28.85
Location of root chord, above axis		1.65
Ventral fins (V_2):		
Root airfoil section	NACA 65A005	
Tip airfoil section	NACA 65A003	
Root chord		6.21
Tip chord		1.28
Semispan, exposed		3.35
Area, exposed, both		17.74
Aspect ratio, each		1.27
Taper ratio, exposed		0.33
Sweepback, leading edge, deg		50
Sweepback, $c/4$, deg		45
Cathedral, deg		70
Location of root chord, longitudinal		24.05
Location of root chord, above axis		0.87
Fuselage (B):		
Length, in.		38.04
Frontal area, sq in.		13.60
Fineness ratio		9.17

TABLE II.- SUMMARY OF TESTS AND CONFIGURATIONS

(a) Basic data

Figure	Description	Configuration
7	Addition of tails	SBW, SBWV ₁ H
8	Natural and fixed transition	SBWV ₁ V ₂ H
9	{ Rocket-motor fairing	SBWV ₁ V ₂ HR
	{ Fuselage fairing	SBWV ₁ V ₂ HG
10	Stabilizer and speed-brake effectiveness	$i_t = -8^\circ, 60^\circ$
11	{ Missiles removed	BWV ₁ V ₂ H
	{ Missiles removed with cavities removed	BWV ₁ V ₂ H ₁ C
12	Missiles extended	S ^E BWV ₁ V ₂ H

(b) Summary data

Figure	Description
13	Variation of longitudinal stability parameter
14	Pitching-moment-coefficient contribution of tail
15	Variation of stabilizer-effectiveness parameter
16	Pitching-moment-coefficient contribution due to speed brakes
17	Variation of lift-curve slope
18	Variation of minimum-drag coefficient
19	Variation of drag-coefficient rise
20	Drag-coefficient increment due to speed brakes
21	Variation of L/D with lift coefficient
22	Variation of $\frac{C_L^{1/2}}{C_D}$
23	Comparison of transonic and supersonic test results

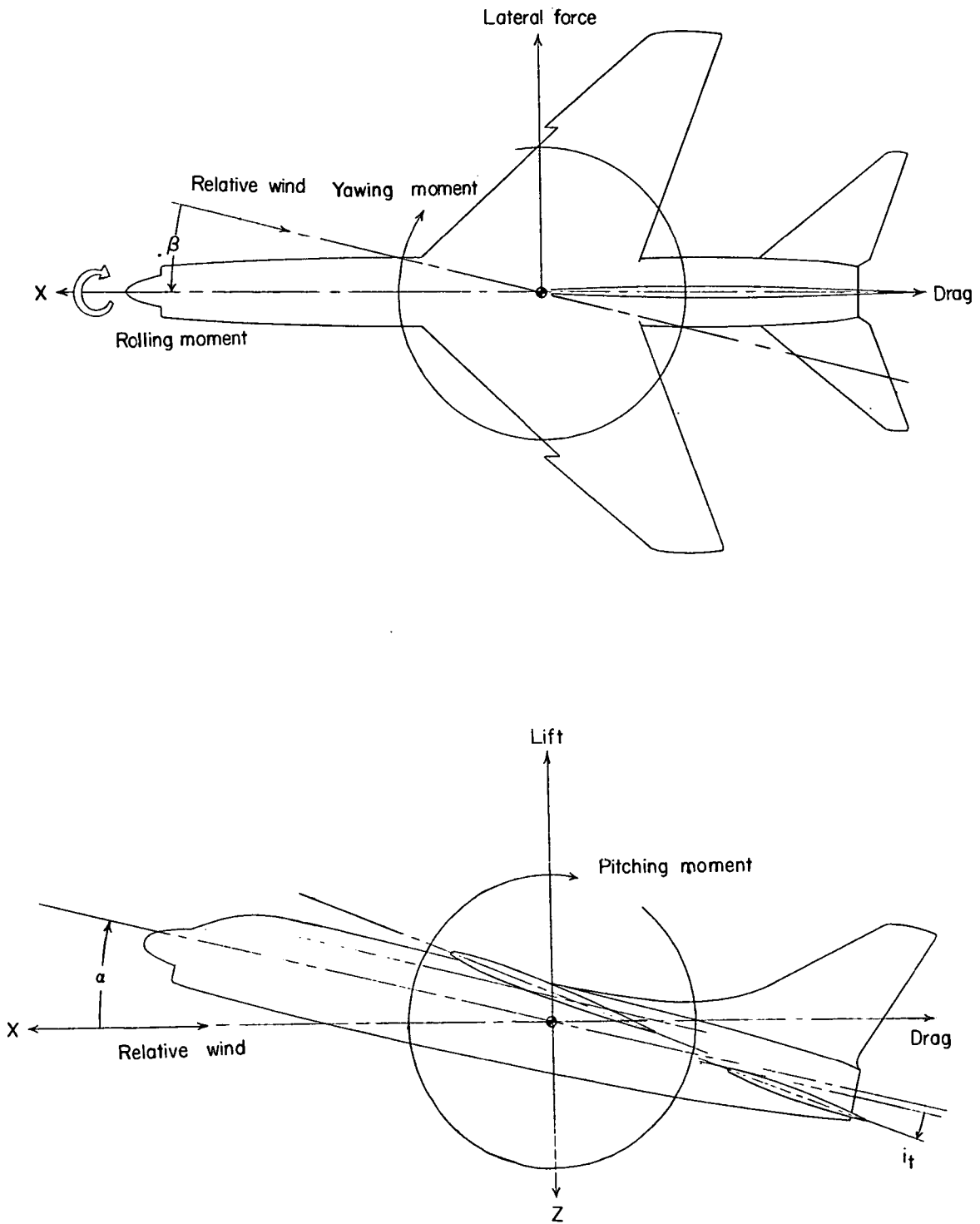


Figure 1.- Coordinate system of stability axes used.

CONFIDENTIAL

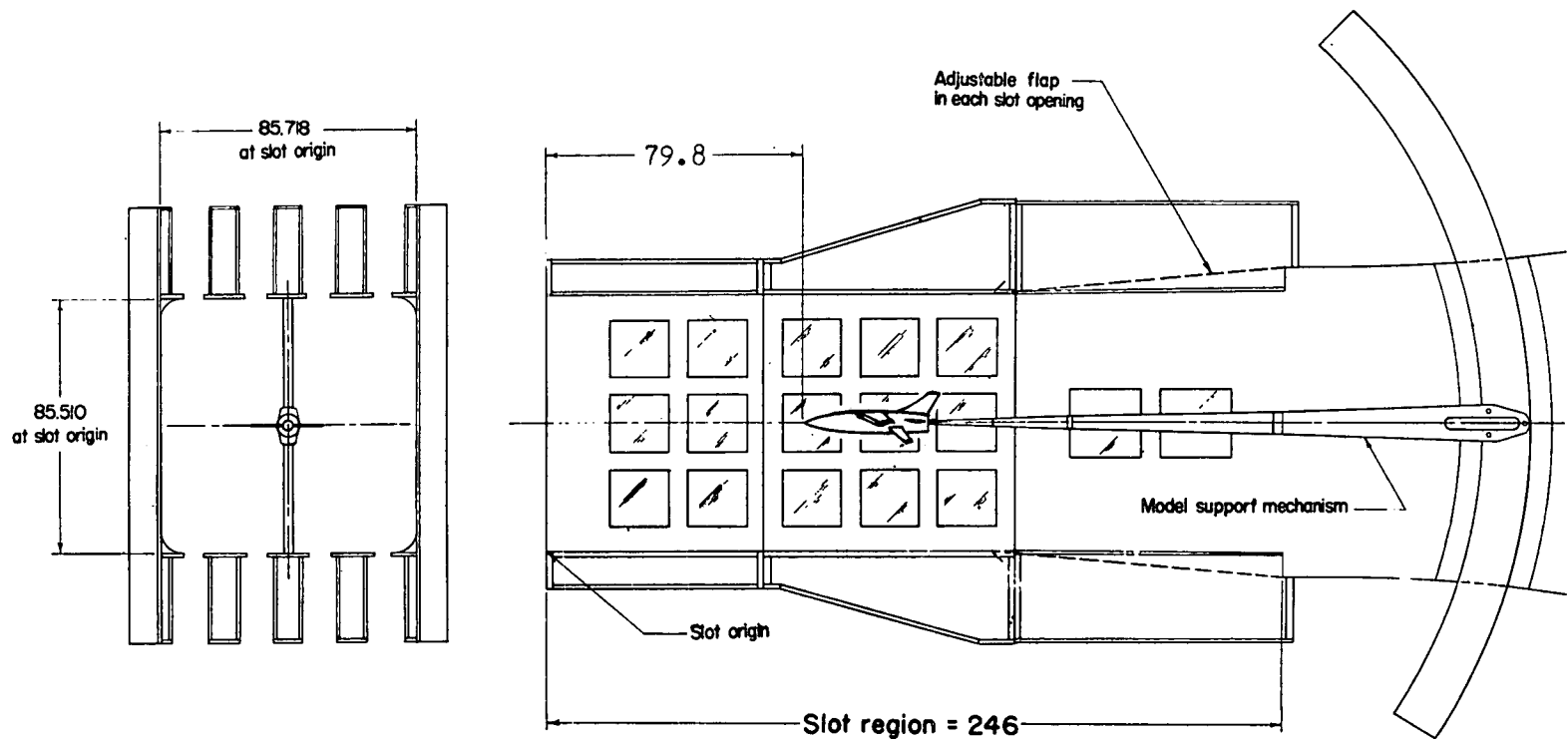


Figure 2.- Details of test section and location of model in the Langley 8-foot transonic pressure tunnel. All dimensions are in inches.

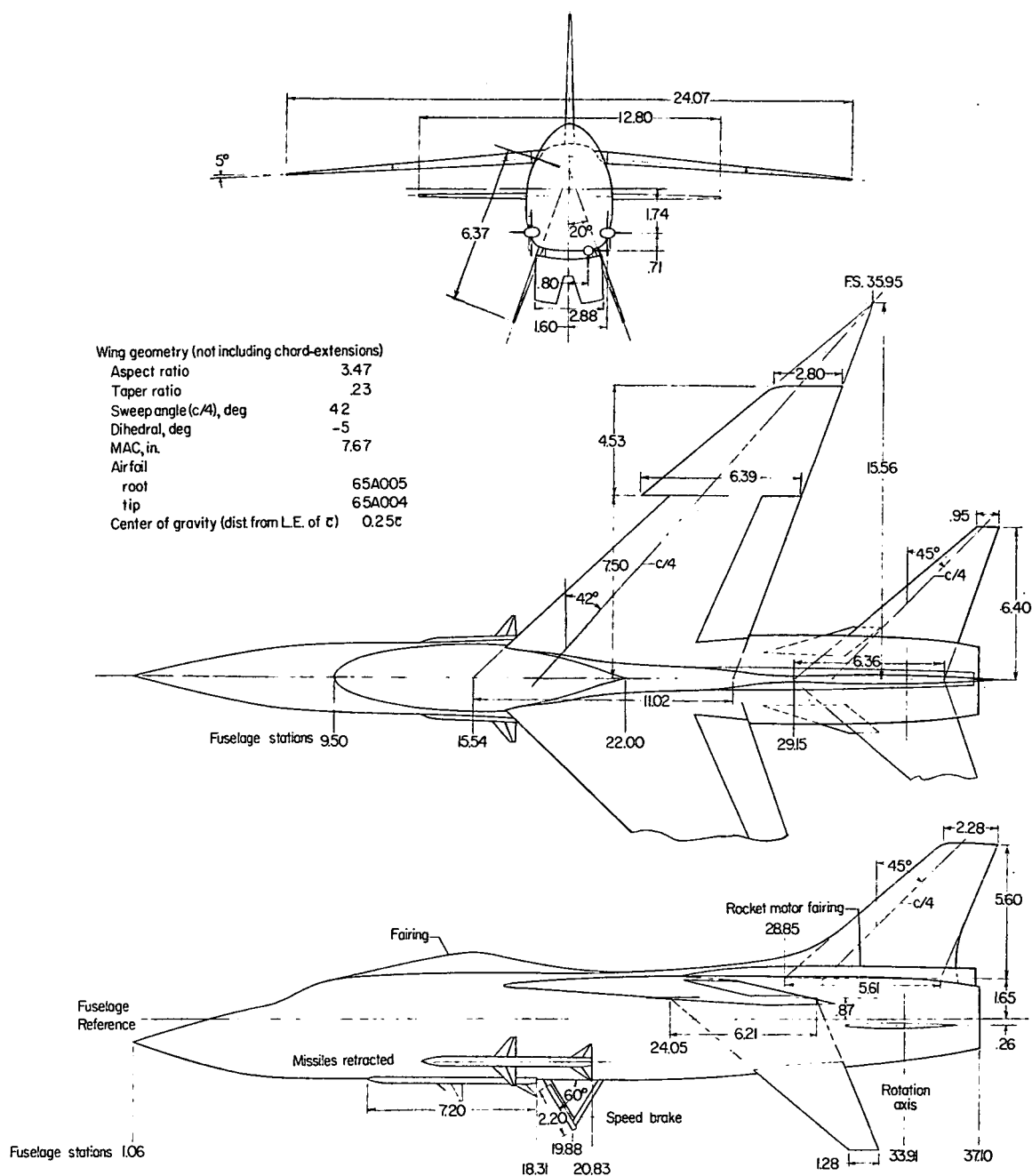


Figure 3.- Three-view drawing of the Chance Vought XF8U-3 airplane model. All dimensions are in inches.

CONFIDENTIAL

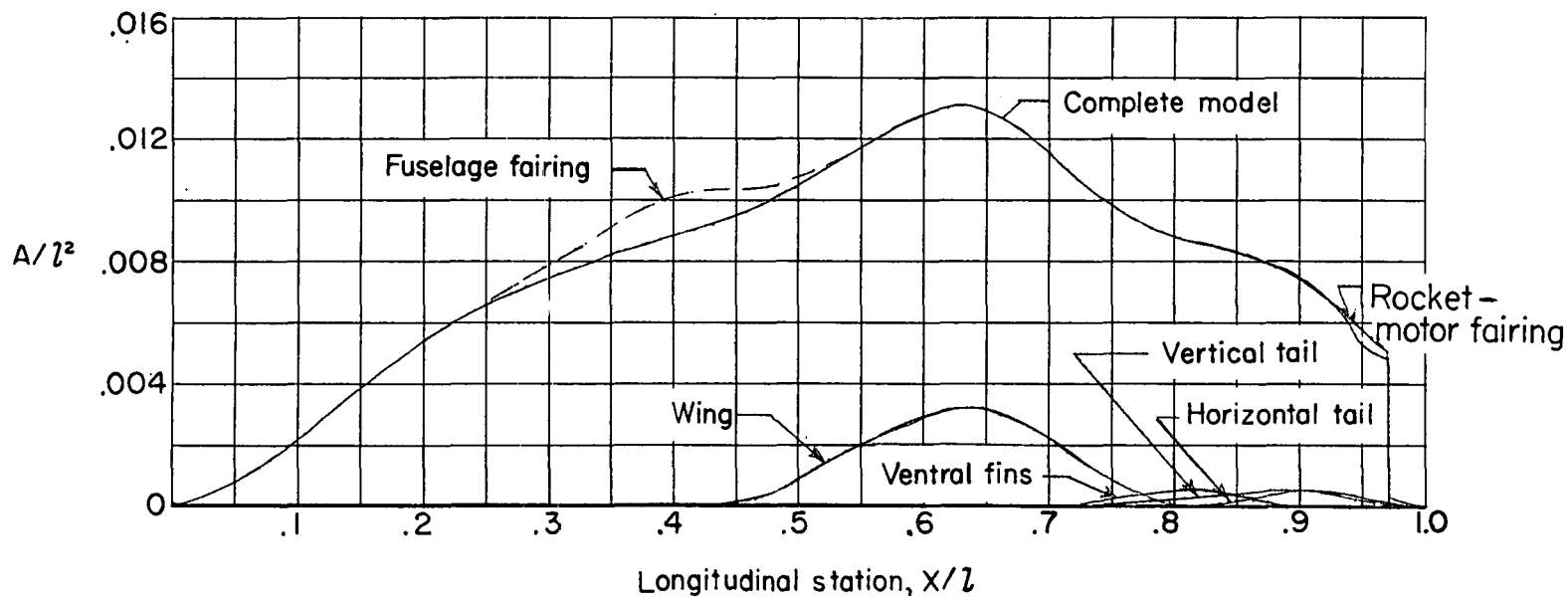
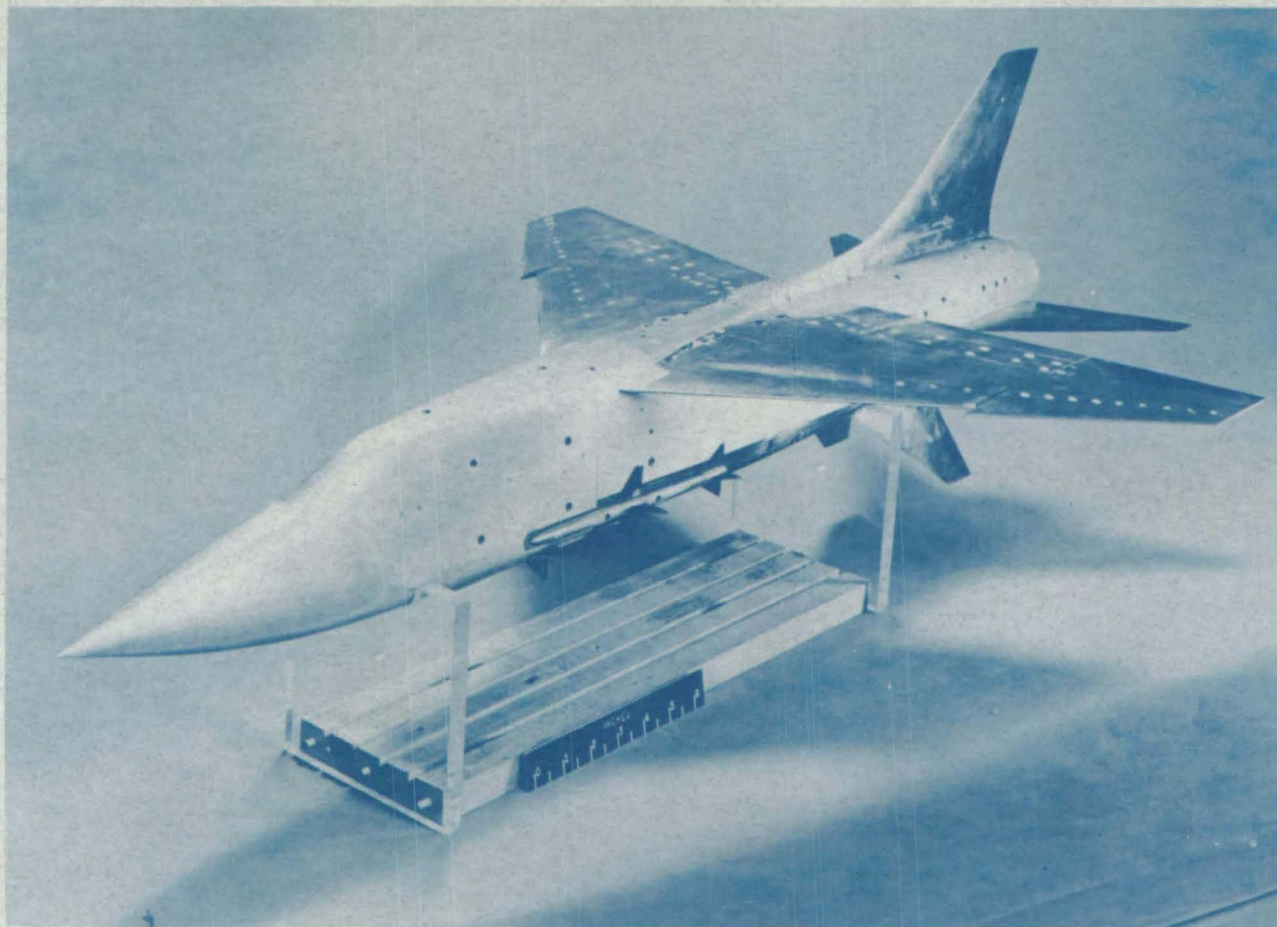


Figure 4.- Area distributions normal to fuselage reference axis of 0.05-scale model of the Chance Vought XF8U-3 airplane.

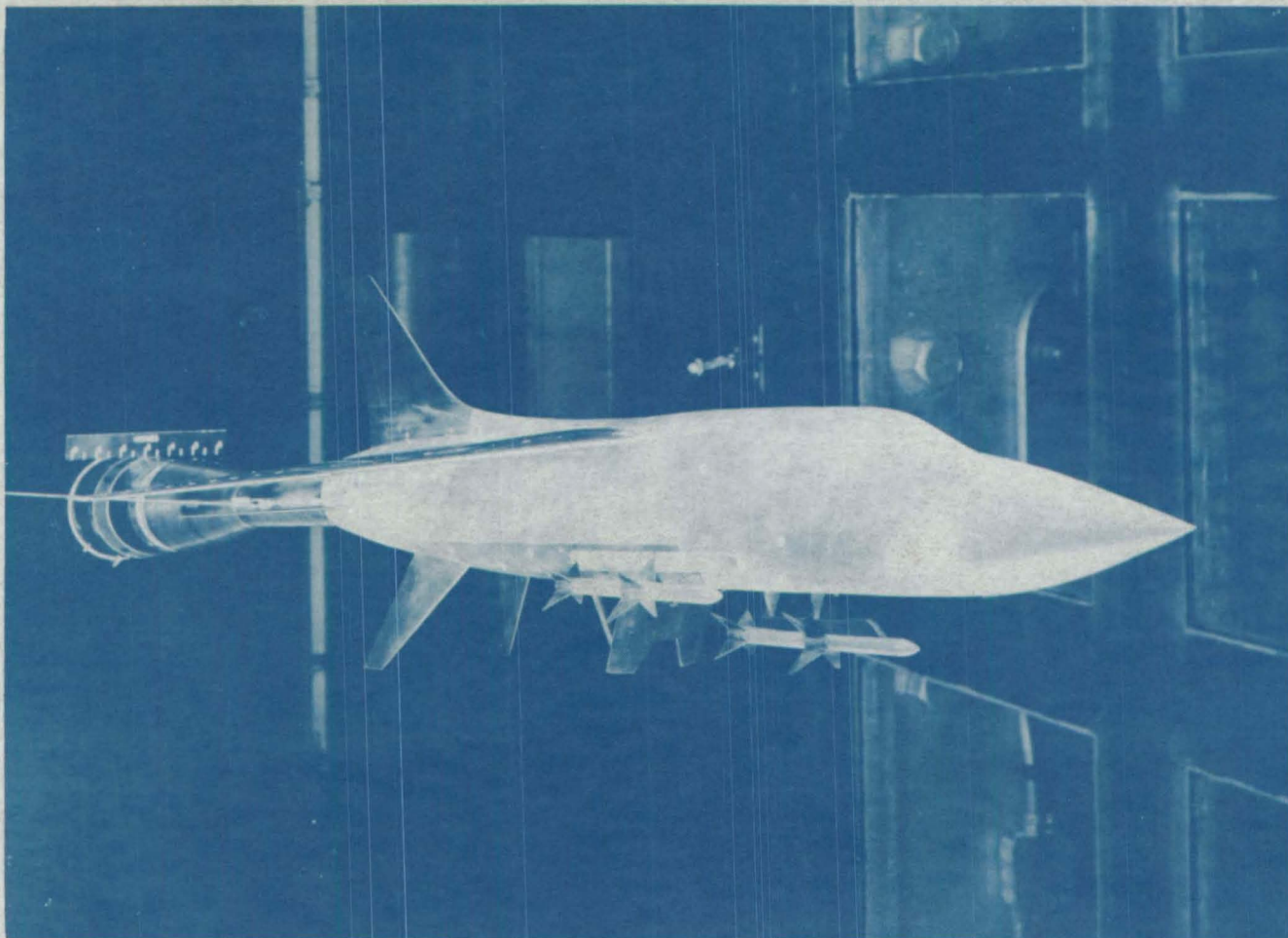
CONFIDENTIAL



(a) Three-quarter front view of complete model with missiles retracted. L-57-246

Figure 5.- Photographs of several model configurations.

CONFIDENTIAL

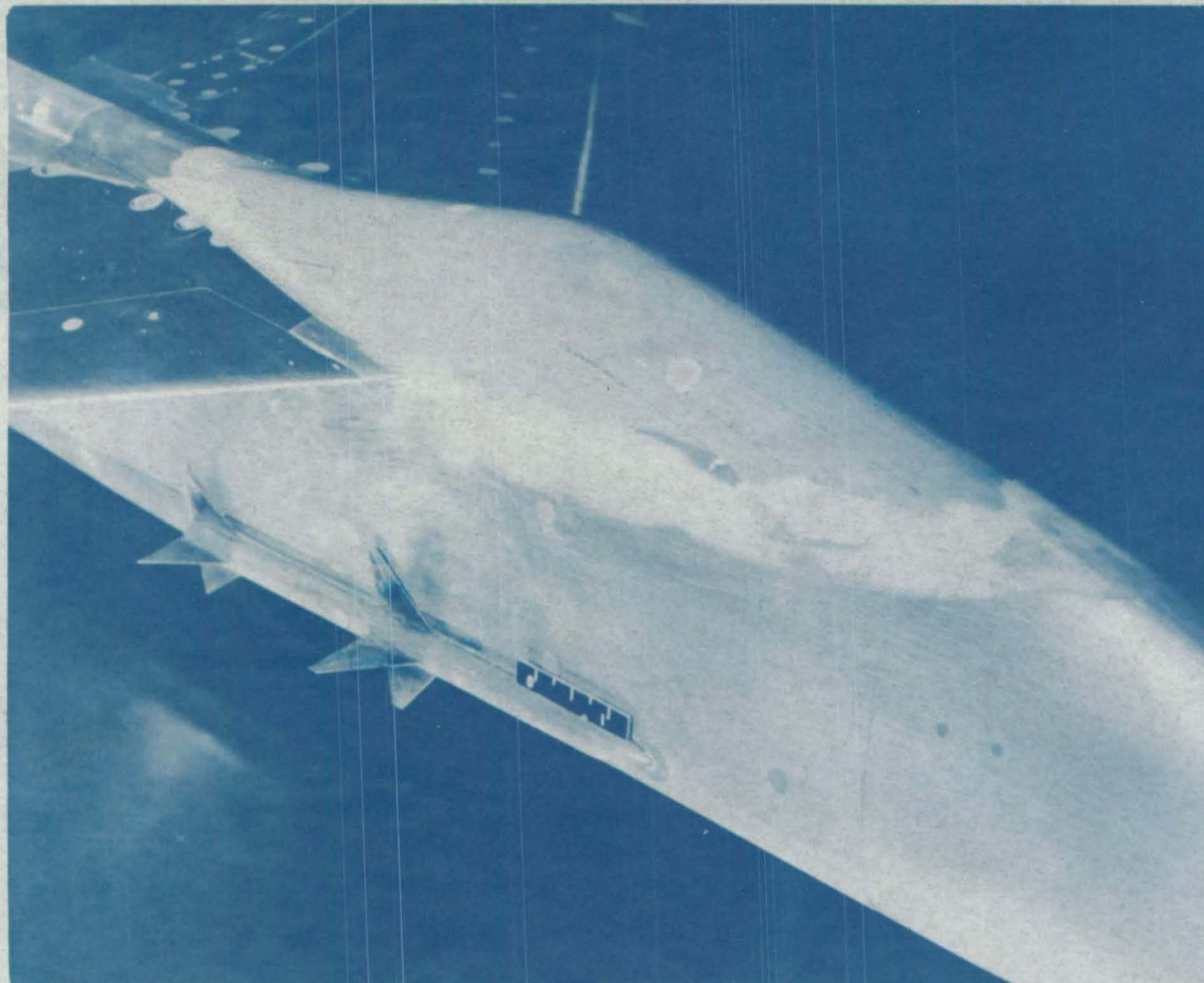


L-57-378

(b) Three-quarter front view of model installed in the Langley 8-foot transonic pressure tunnel; missiles extended and speed brakes deflected 60°.

Figure 5.- Continued.

CONFIDENTIAL



(c) Closeup view of fairing attached to top of fuselage. L-57-590

Figure 5.- Concluded.

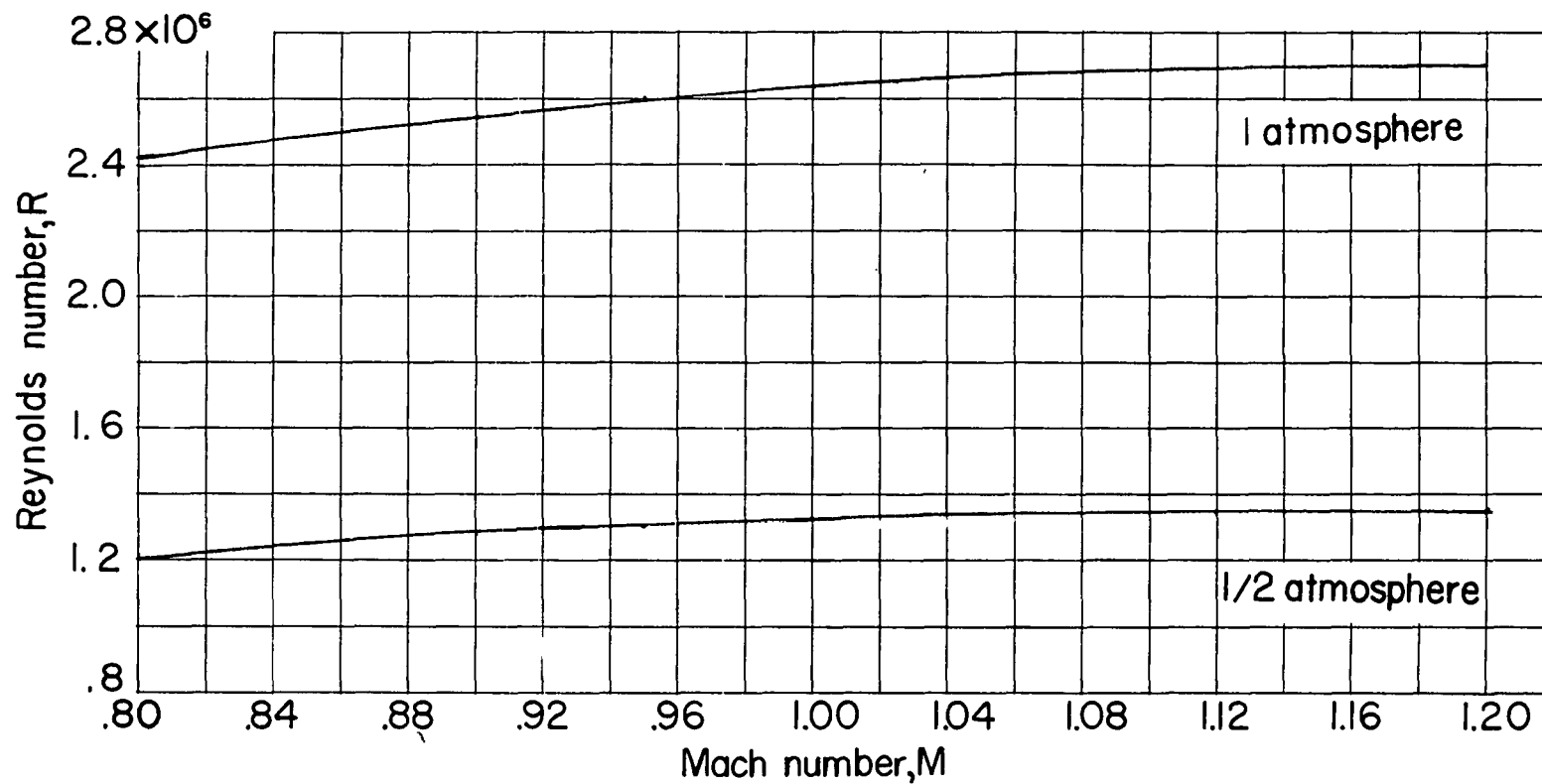
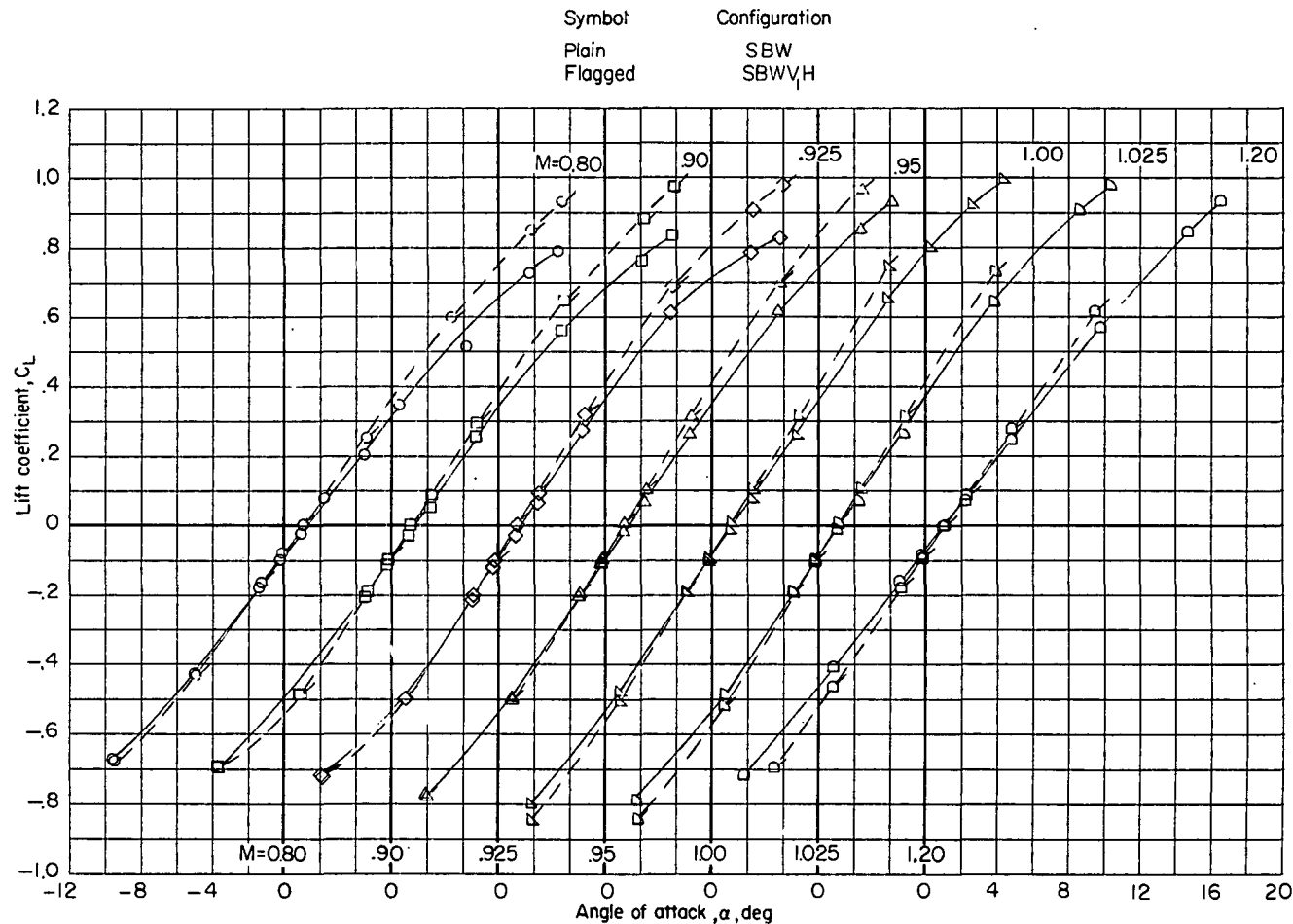


Figure 6.- Average Reynolds numbers as a function of test Mach number based on wing mean aerodynamic chord.

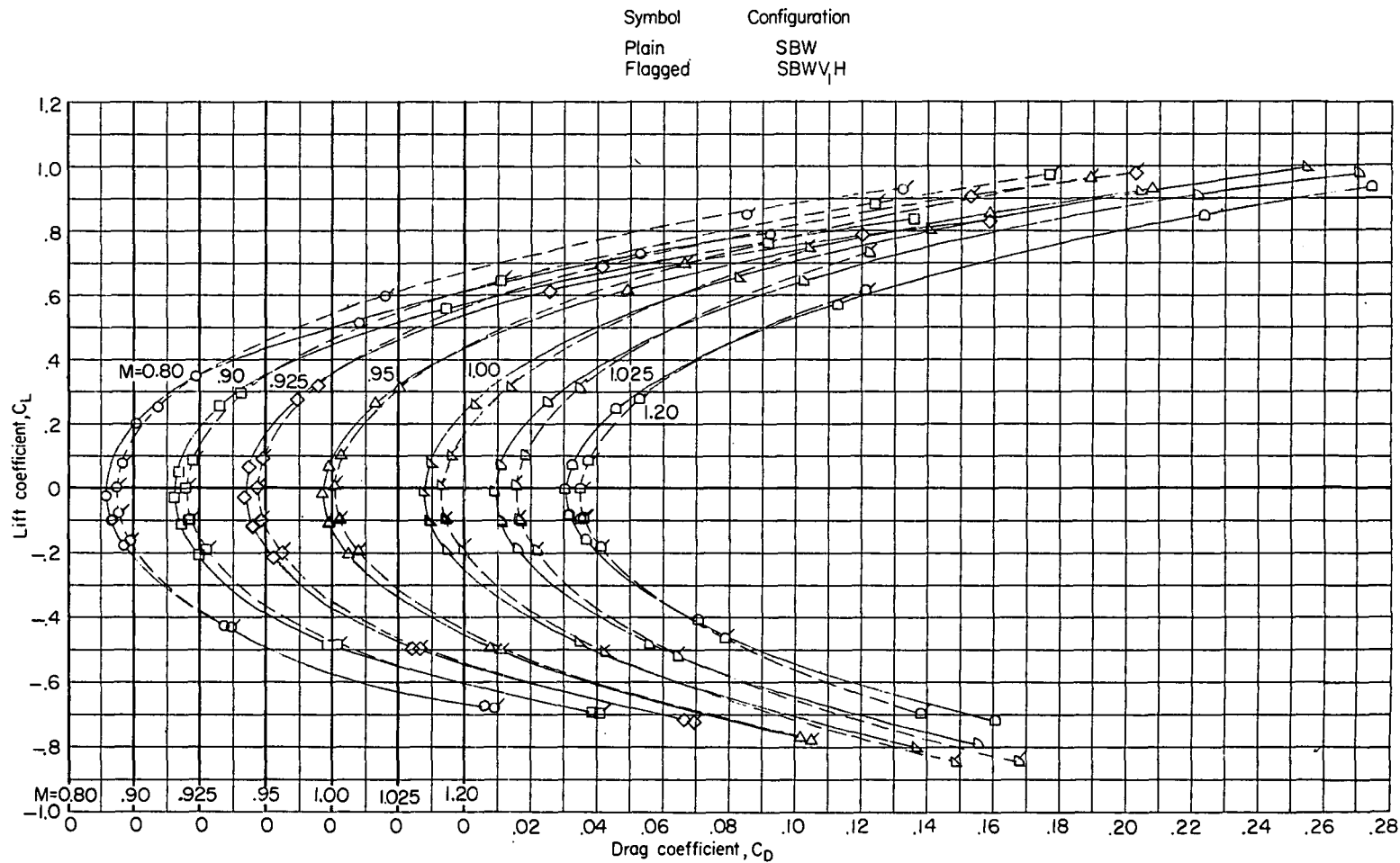
CONFIDENTIAL



(a) Angle of attack.

Figure 7.- Comparison of longitudinal-stability characteristics of the tail-off (SBW) and basic tail-on (SBWV₁H) configuration. $i_t = 0^\circ$.

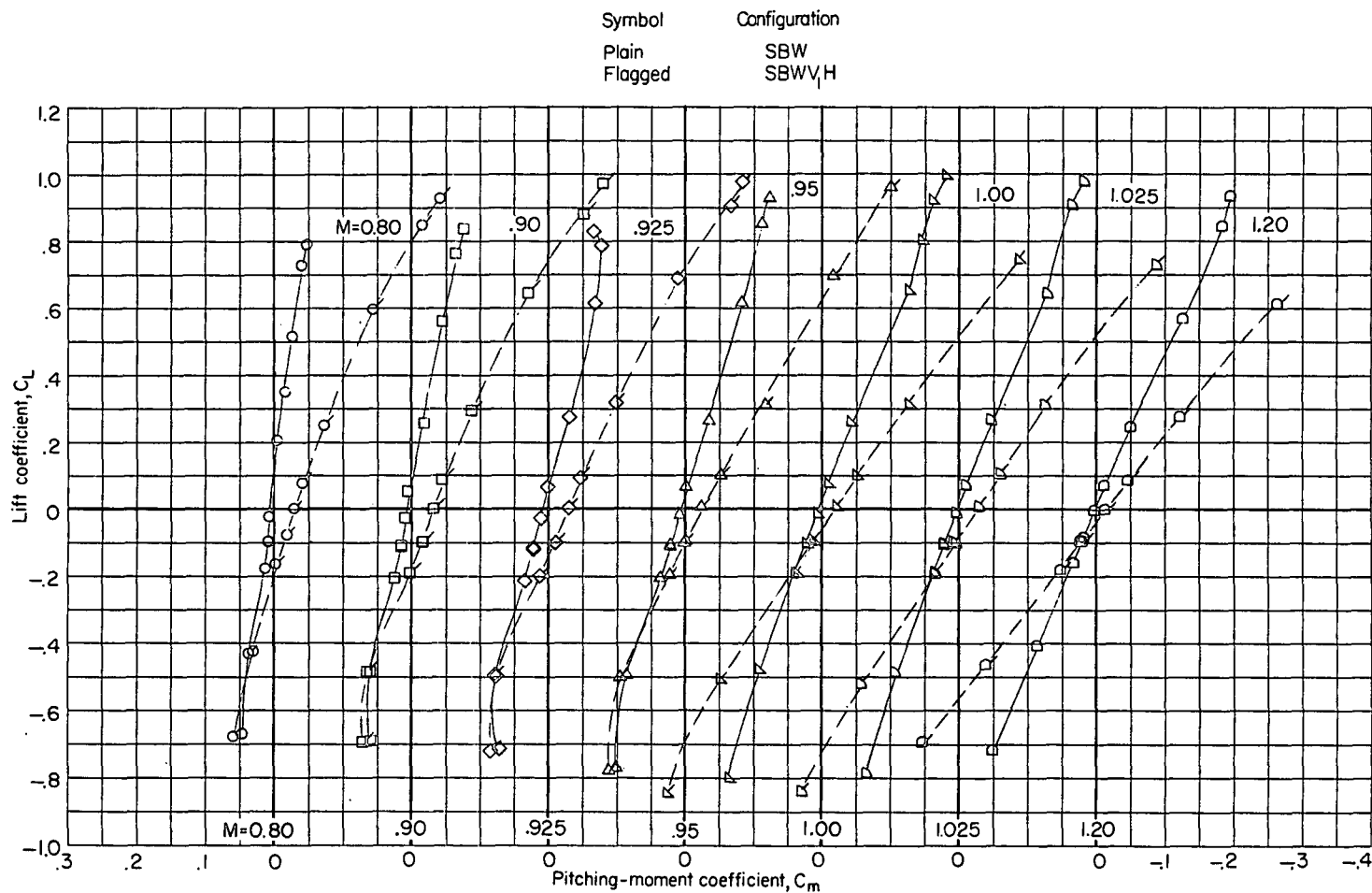
CONFIDENTIAL



(b) Drag coefficient.

Figure 7.- Continued.

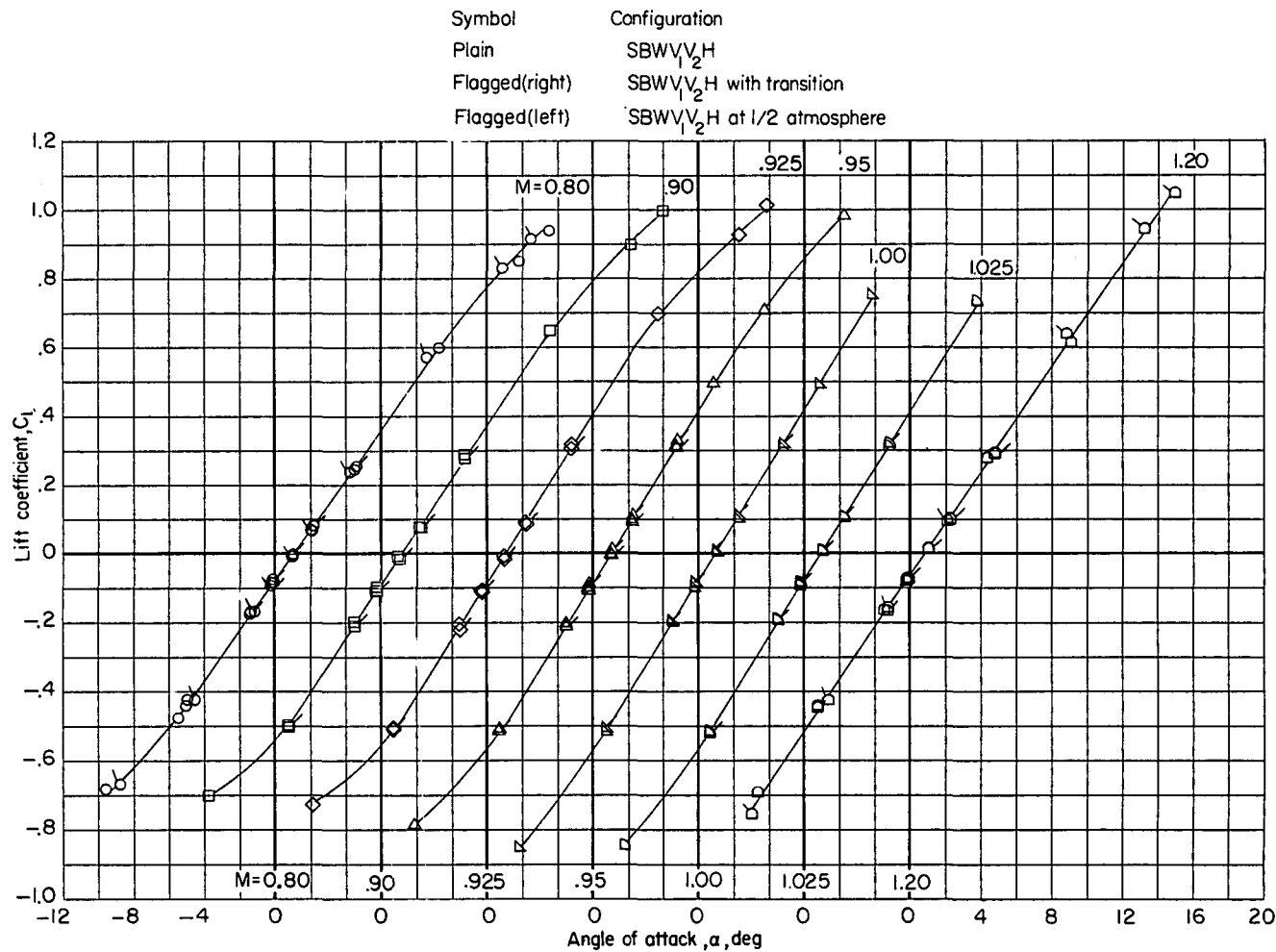
CONFIDENTIAL



(c) Pitching-moment coefficient.

Figure 7.- Concluded.

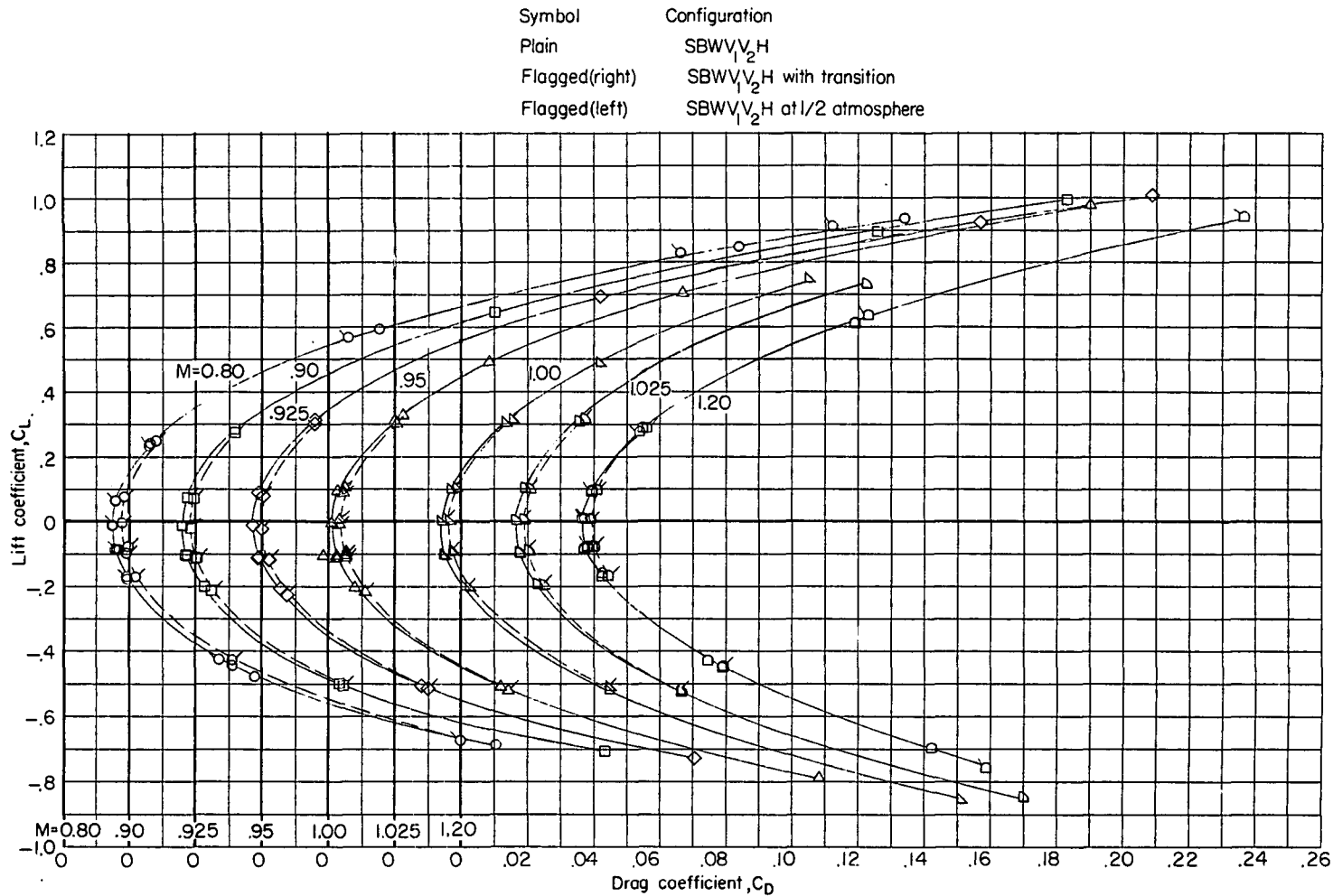
CONFIDENTIAL



(a) Angle of attack.

Figure 8.- Effect of fixed transition on longitudinal-stability characteristics of complete model (SBWV₁V₂H). $i_t = 0^\circ$.

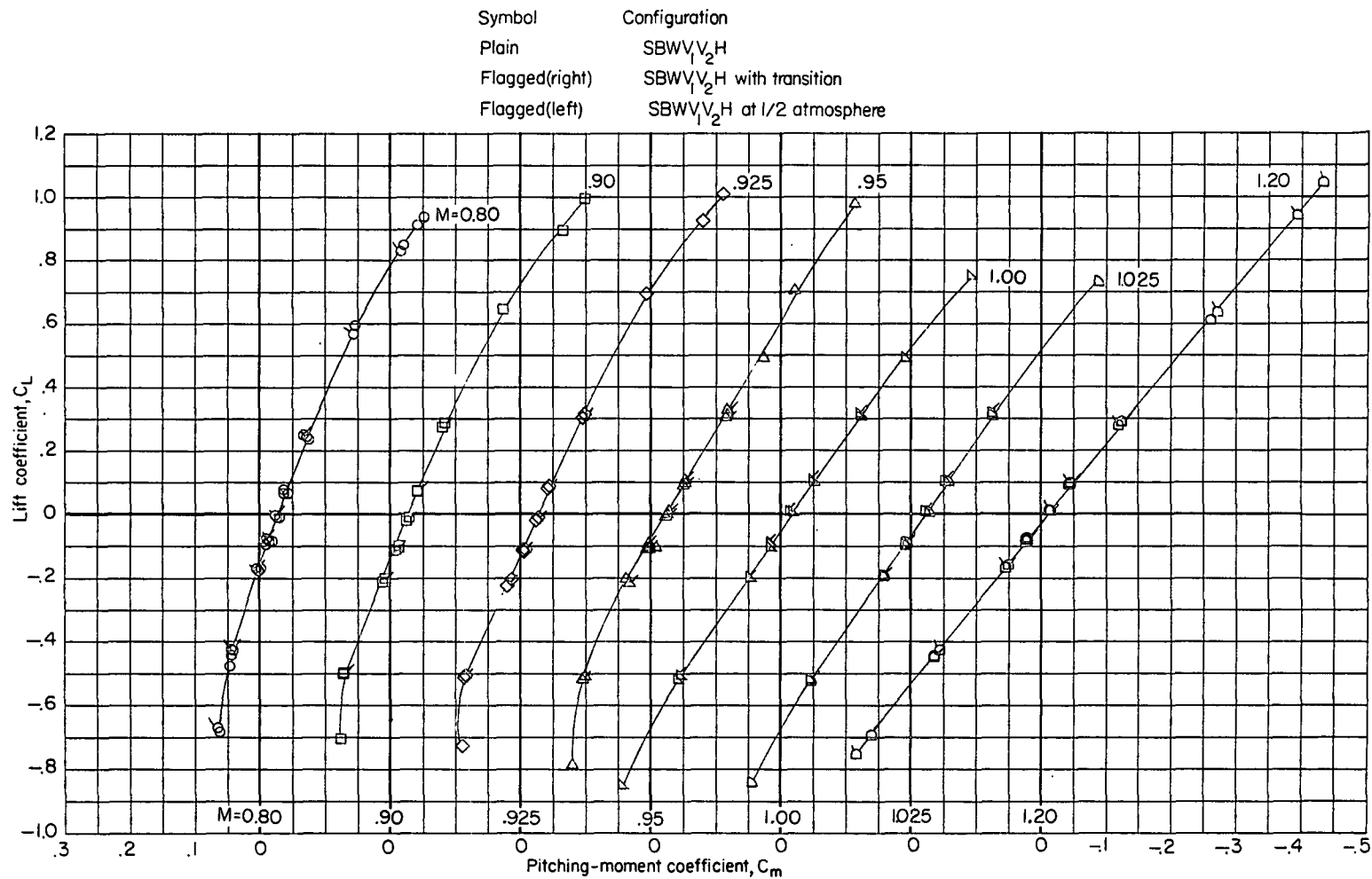
CONFIDENTIAL



(b) Drag coefficient.

Figure 8.- Continued.

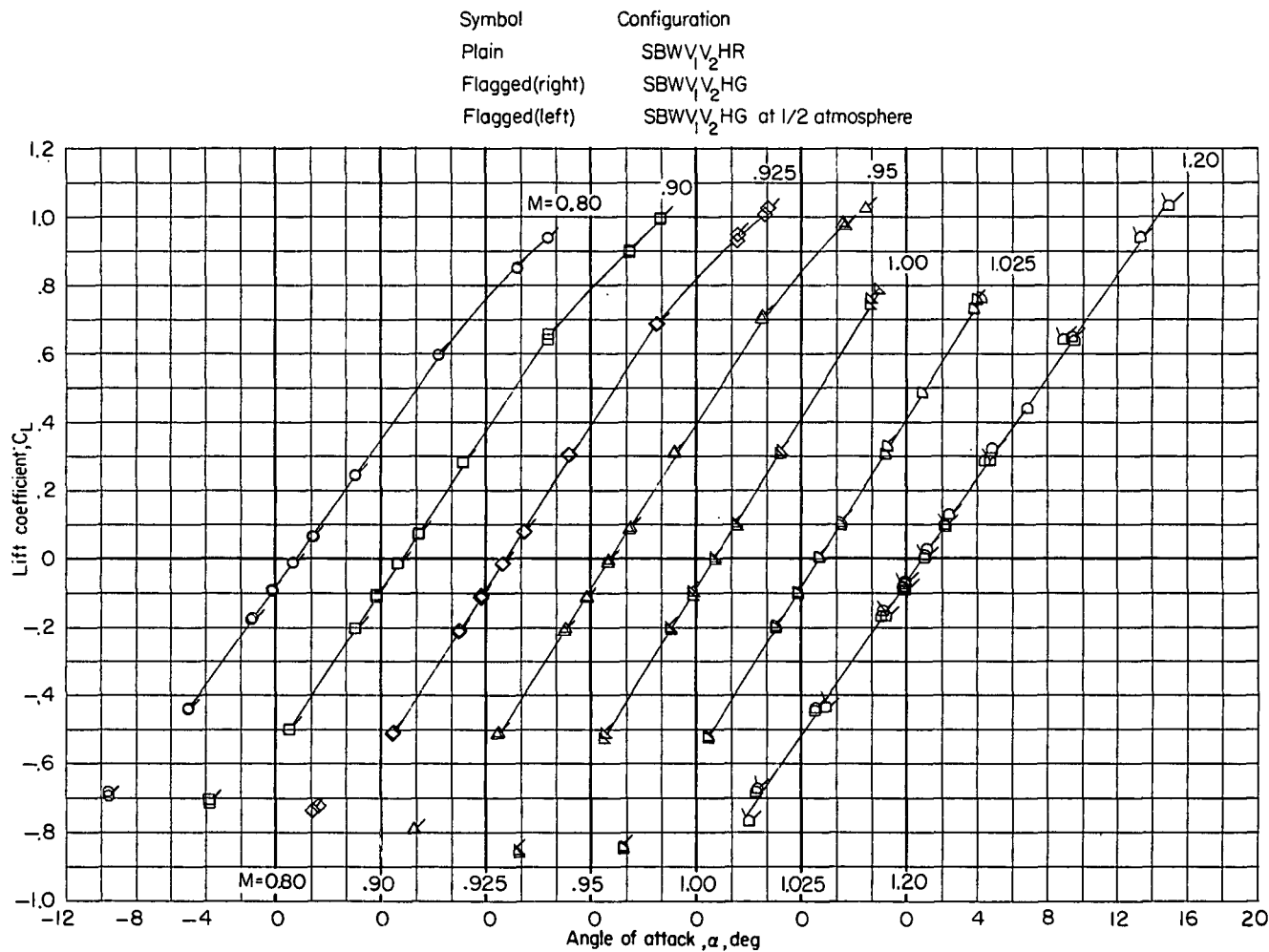
CONFIDENTIAL



(c) Pitching-moment coefficient.

Figure 8.- Concluded.

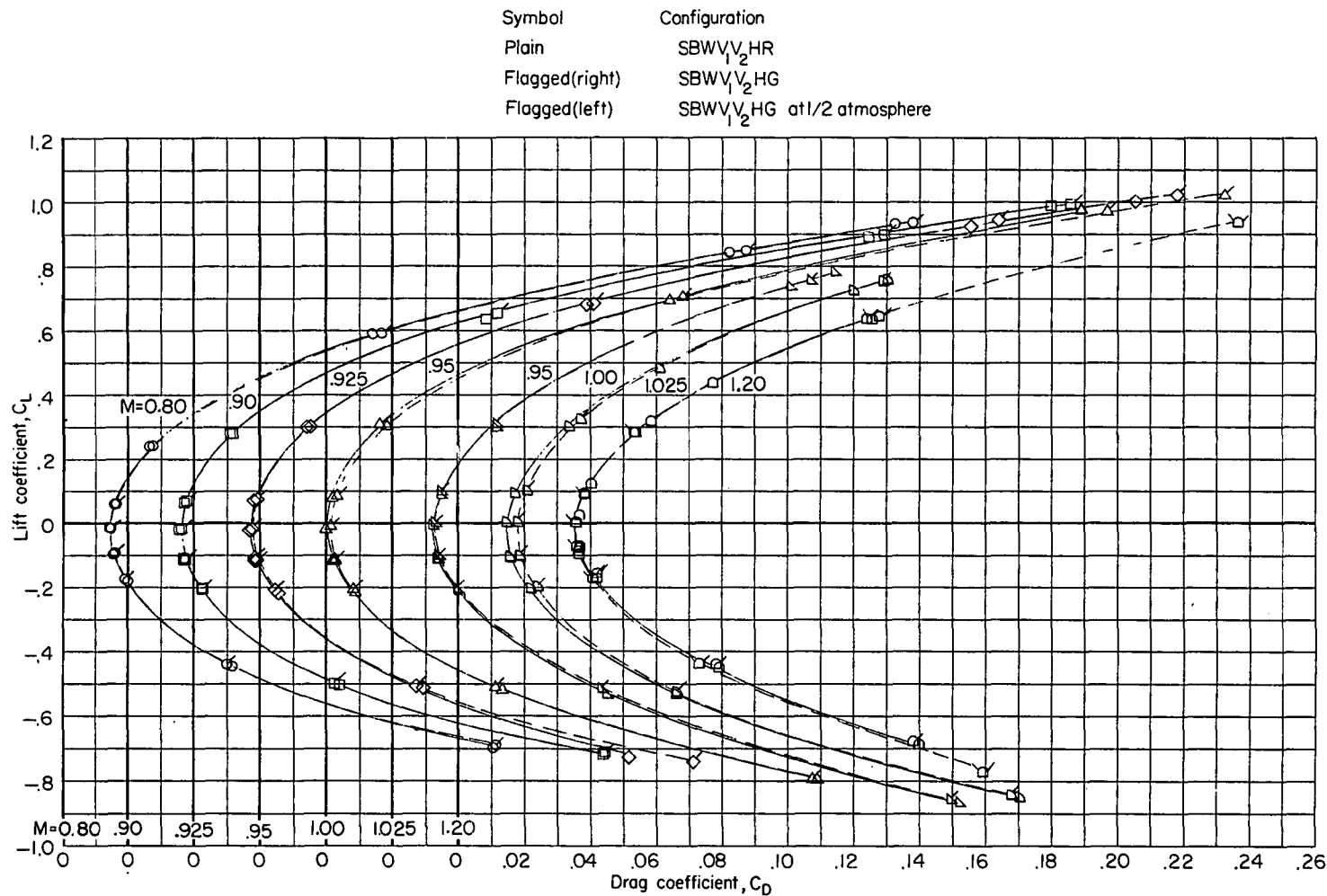
CONFIDENTIAL



(a) Angle of attack.

Figure 9.- Effect on longitudinal-stability characteristics resulting from installation of rocket-motor fairing (SBWV₁V₂HR) or fuselage fairing (SBWV₁V₂HG). $i_t = 0^\circ$.

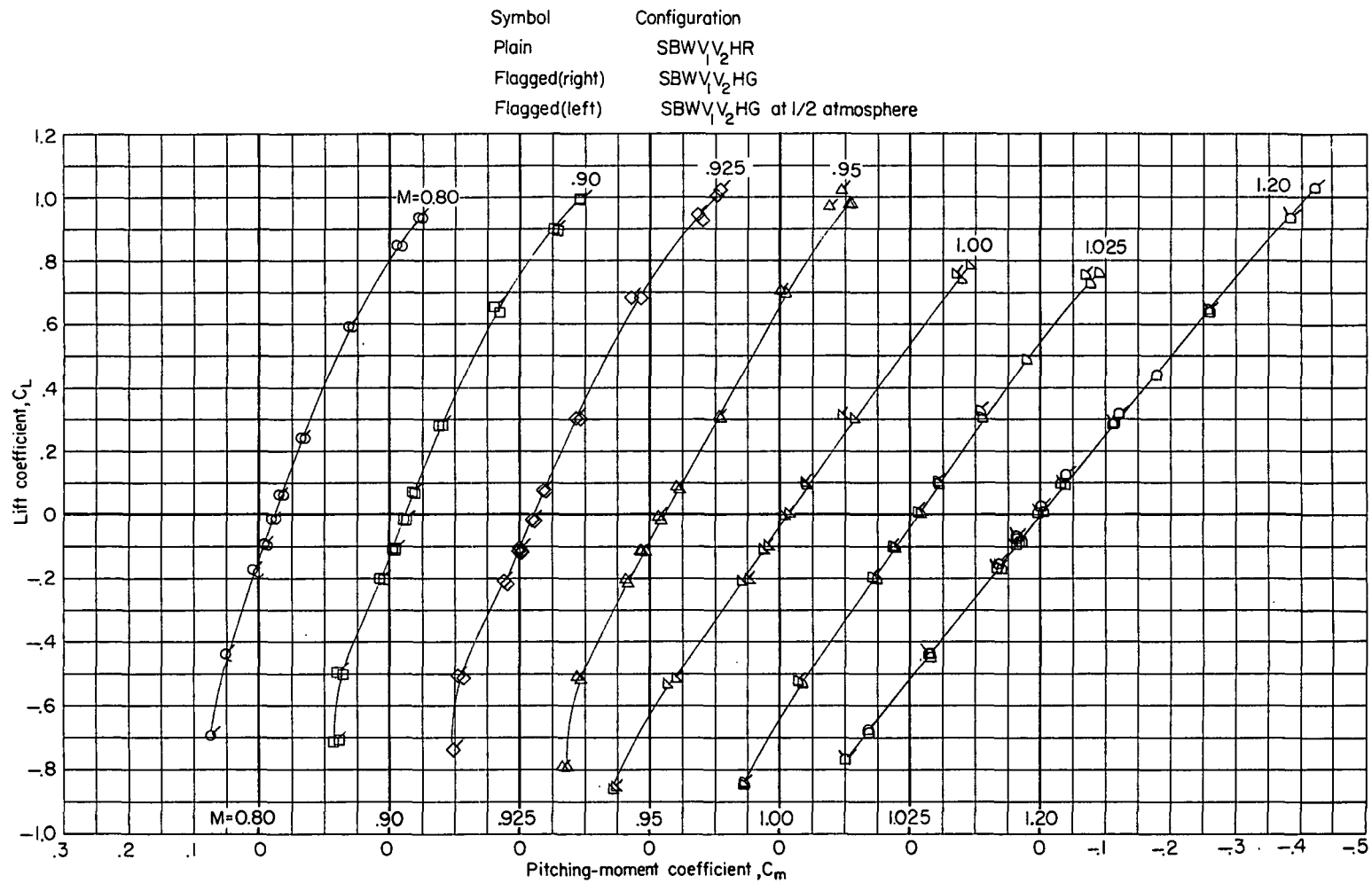
CONFIDENTIAL



(b) Drag coefficient.

Figure 9.- Continued.

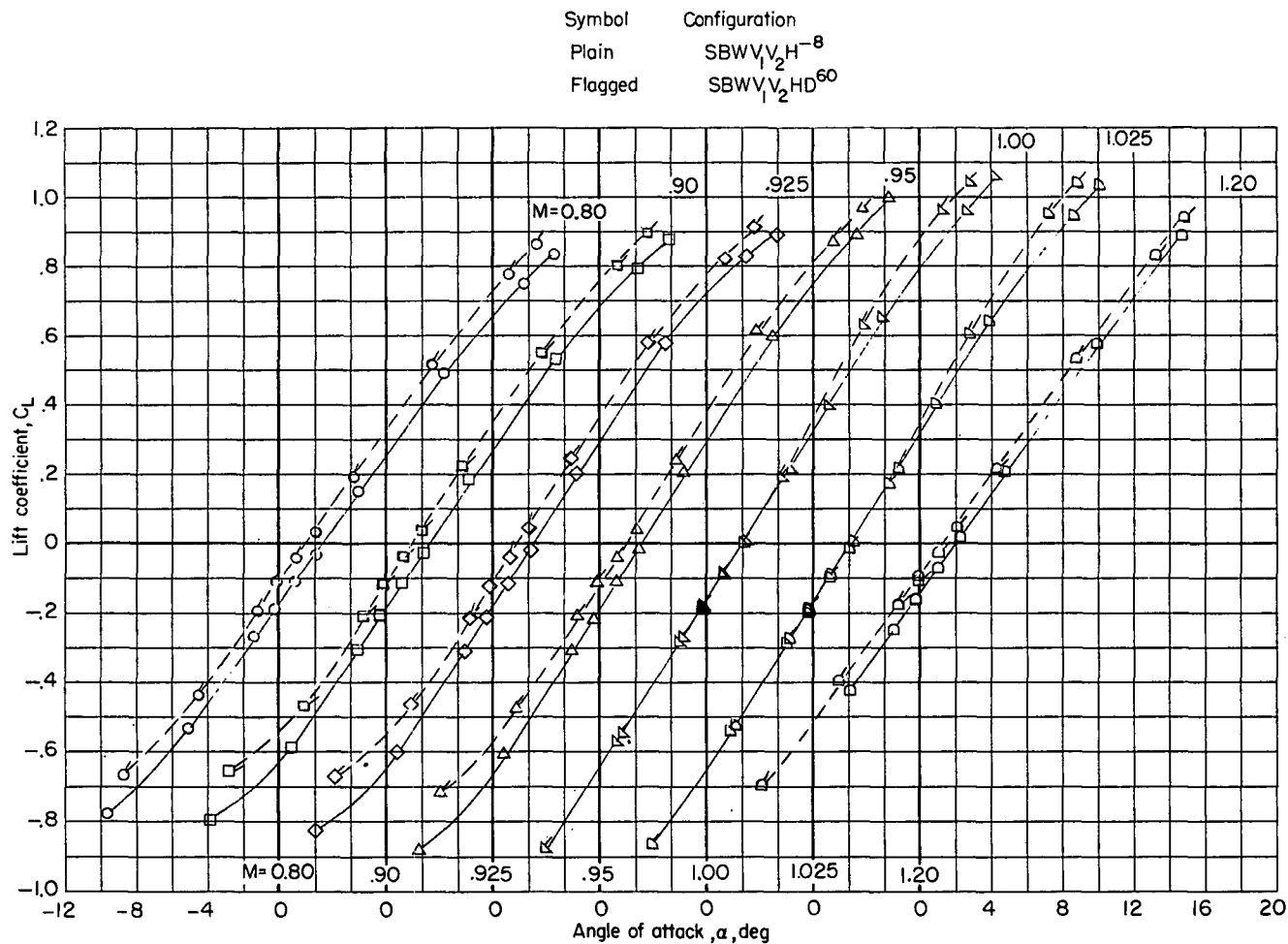
CONFIDENTIAL



(c) Pitching-moment coefficient.

Figure 9.- Concluded.

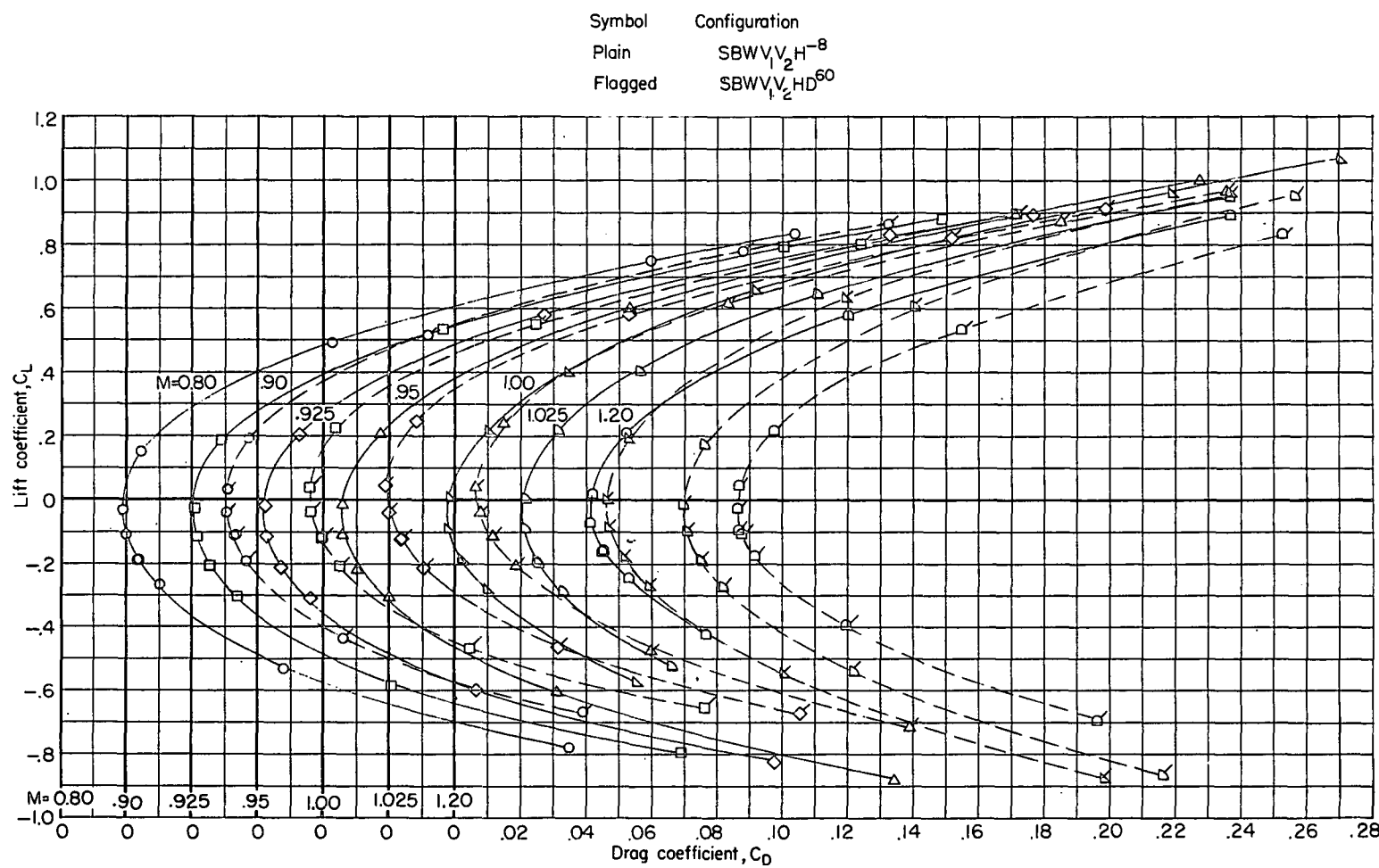
CONFIDENTIAL



(a) Angle of attack.

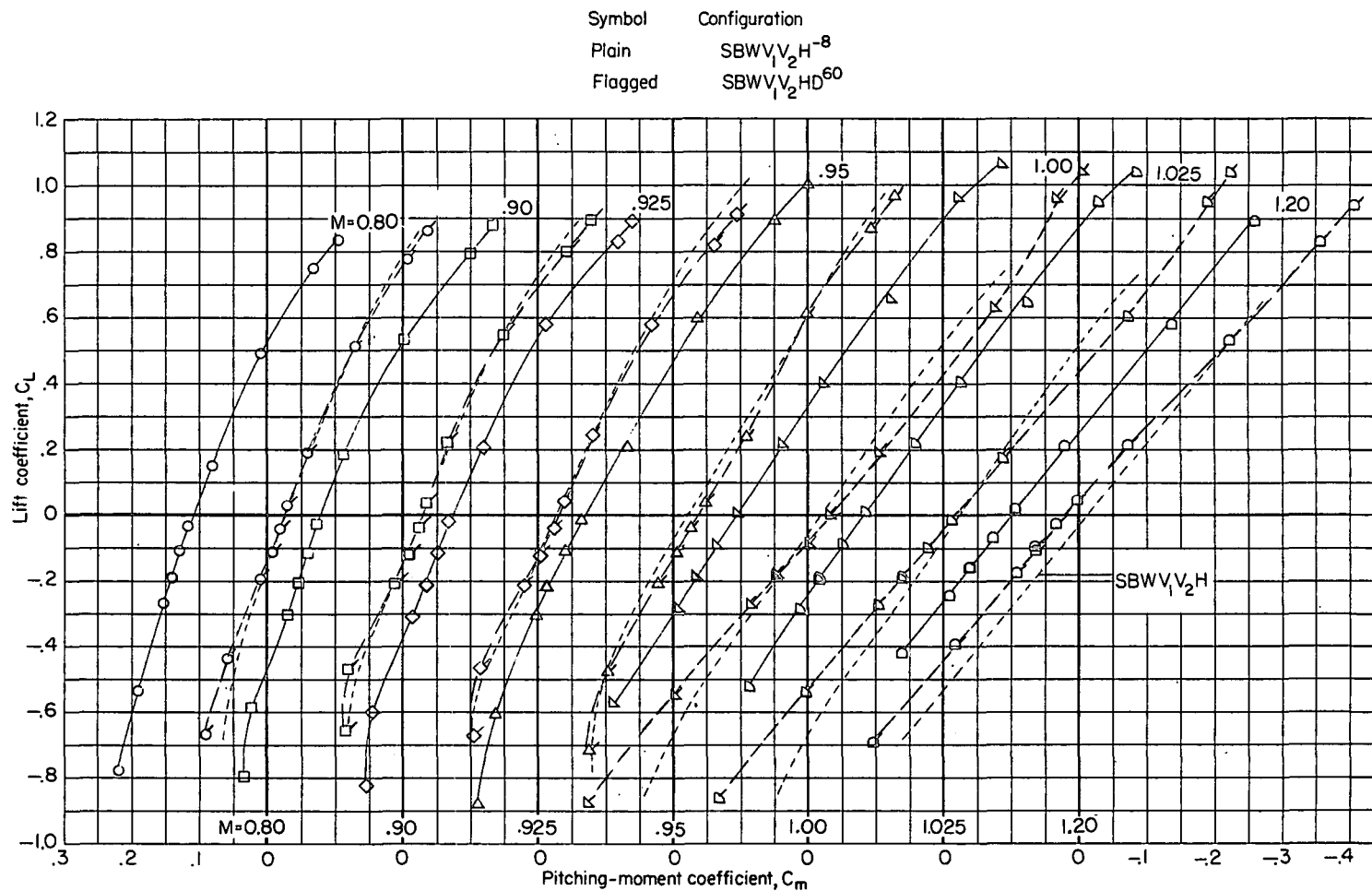
Figure 10.- Effects on longitudinal-stability characteristics due to stabilizer deflection (SBW₁V₂H⁻⁸) or speed-brake deflection (SBW₁V₂HD⁶⁰). $i_t = 0^\circ$.

CONFIDENTIAL



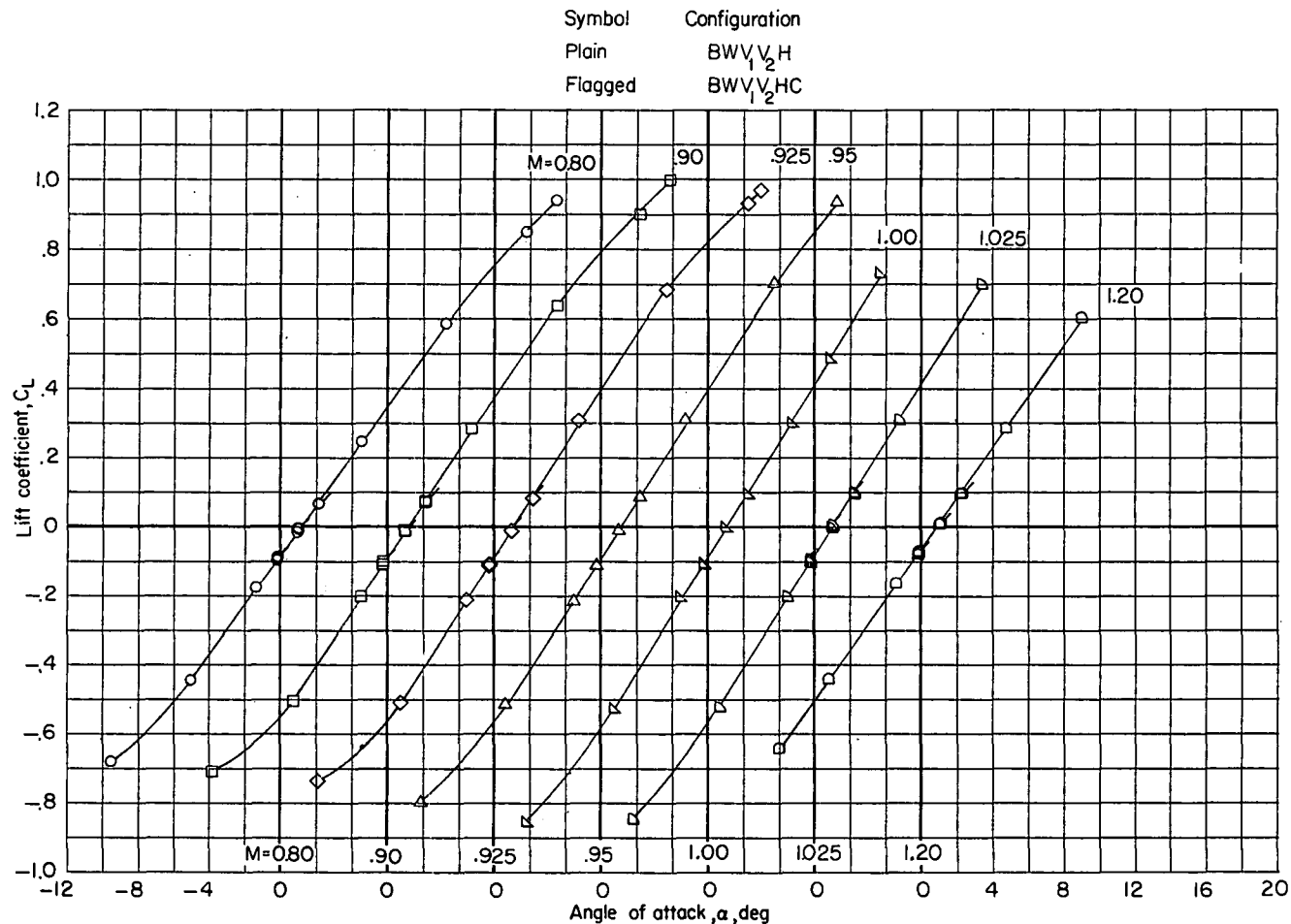
(b) Drag coefficient.

Figure 10.- Continued.



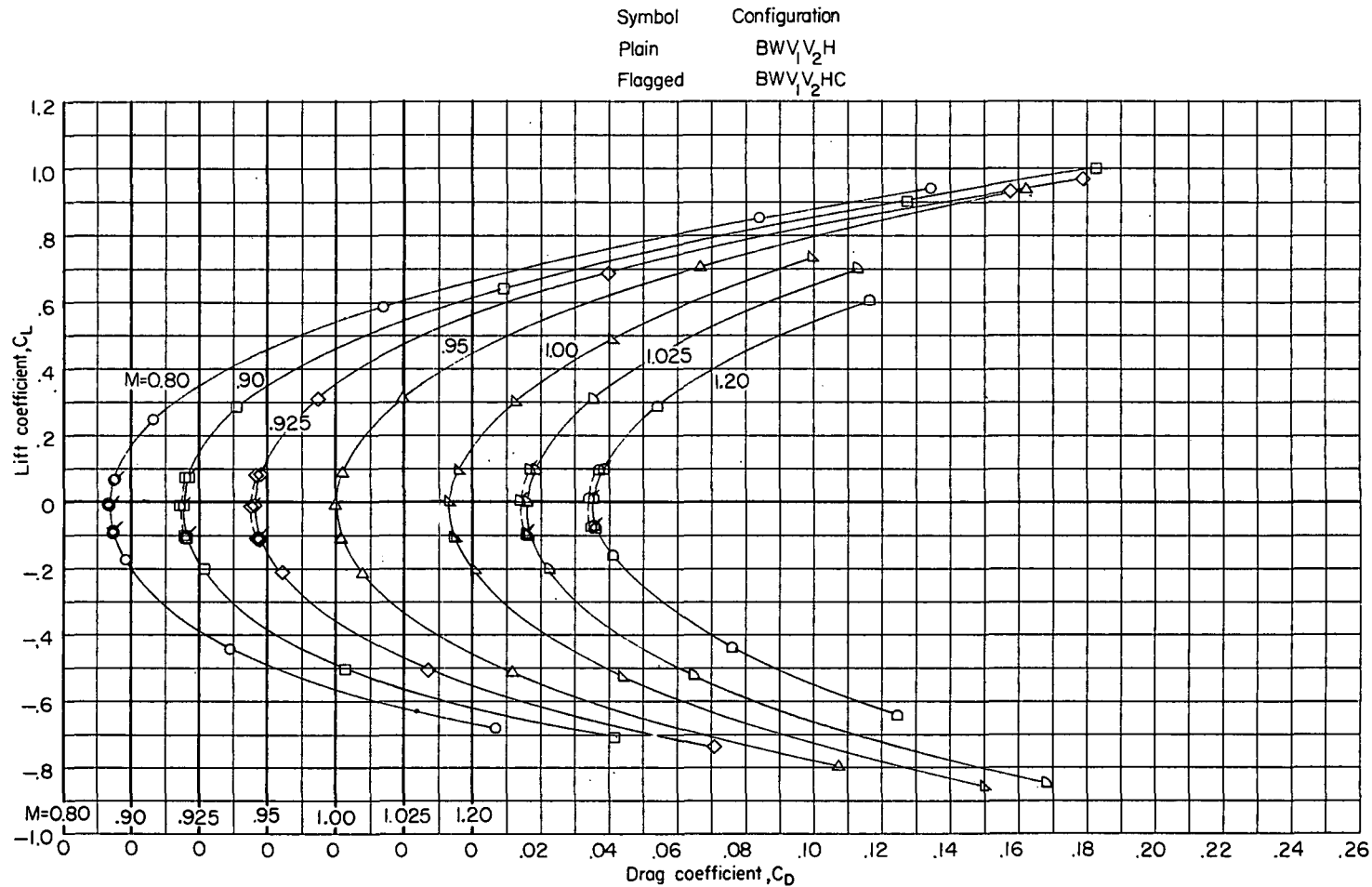
(c) Pitching-moment coefficient.

Figure 10.- Concluded.



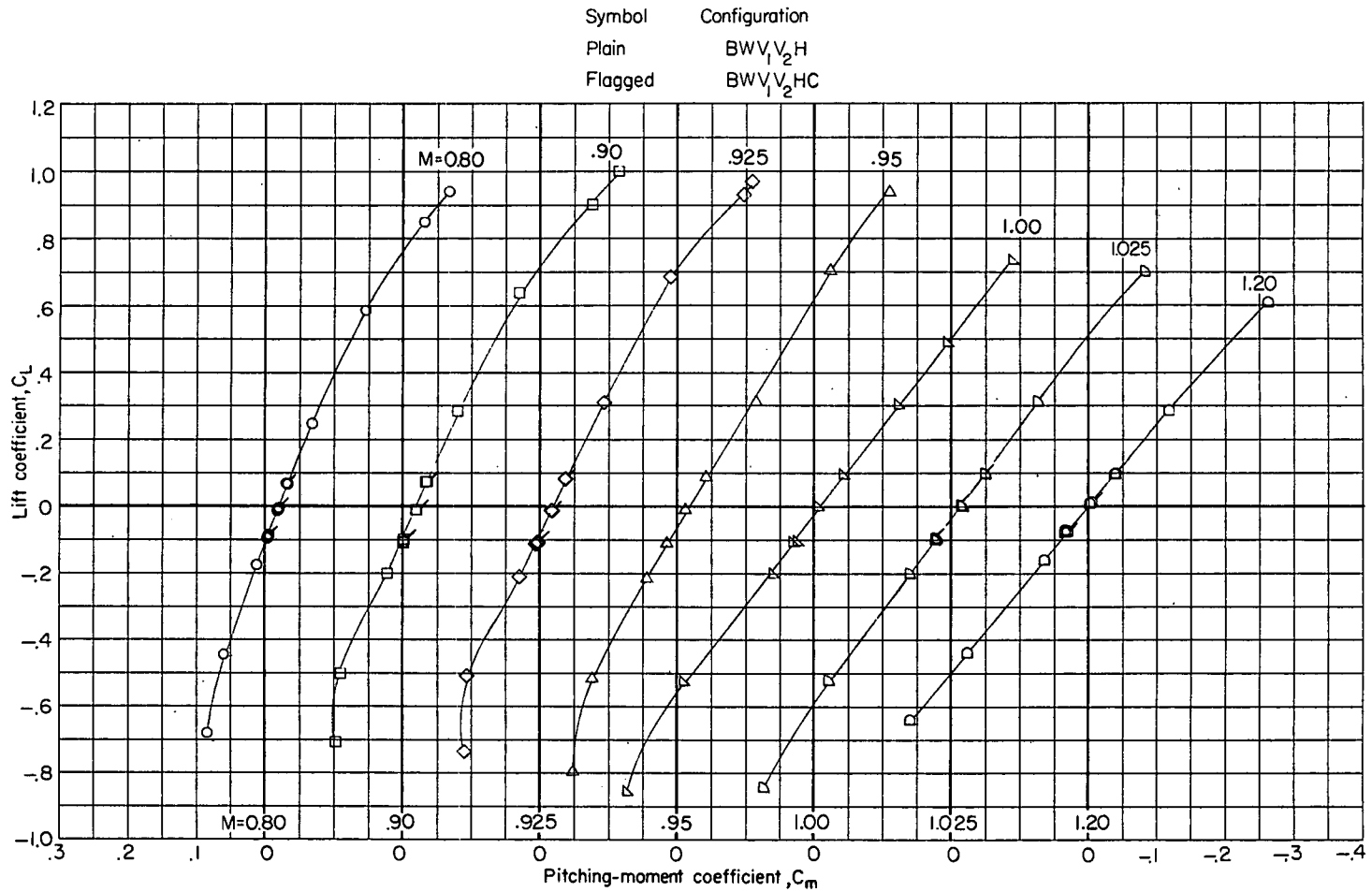
(a) Angle of attack.

Figure 11.- Comparison of longitudinal-stability characteristics for model with missiles removed (BWV₁V₂H), and missiles removed with faired cavities (BWV₁V₂HC). $i_t = 0^\circ$.



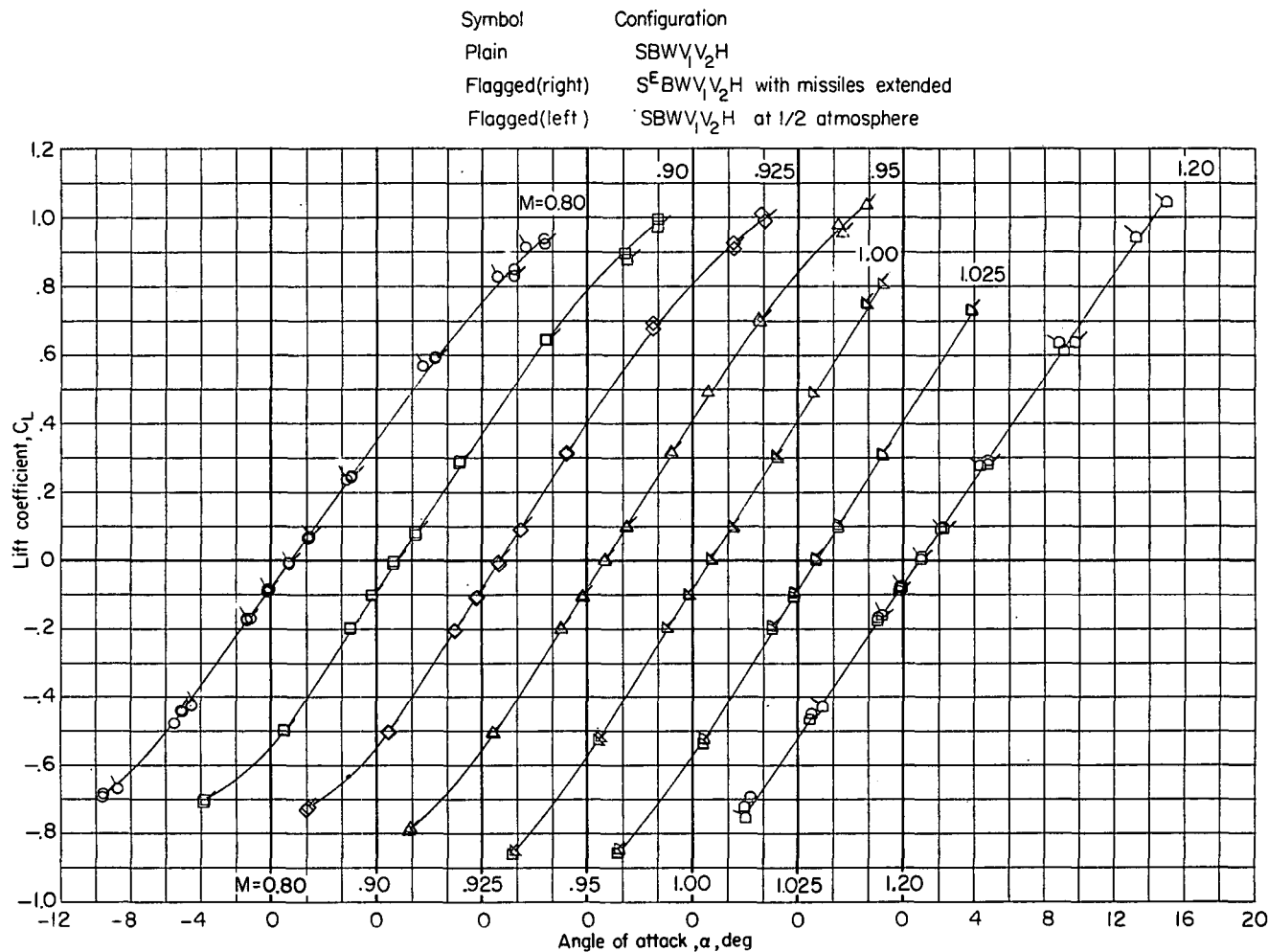
(b) Drag coefficient.

Figure 11.- Continued.



(c) Pitching-moment coefficient.

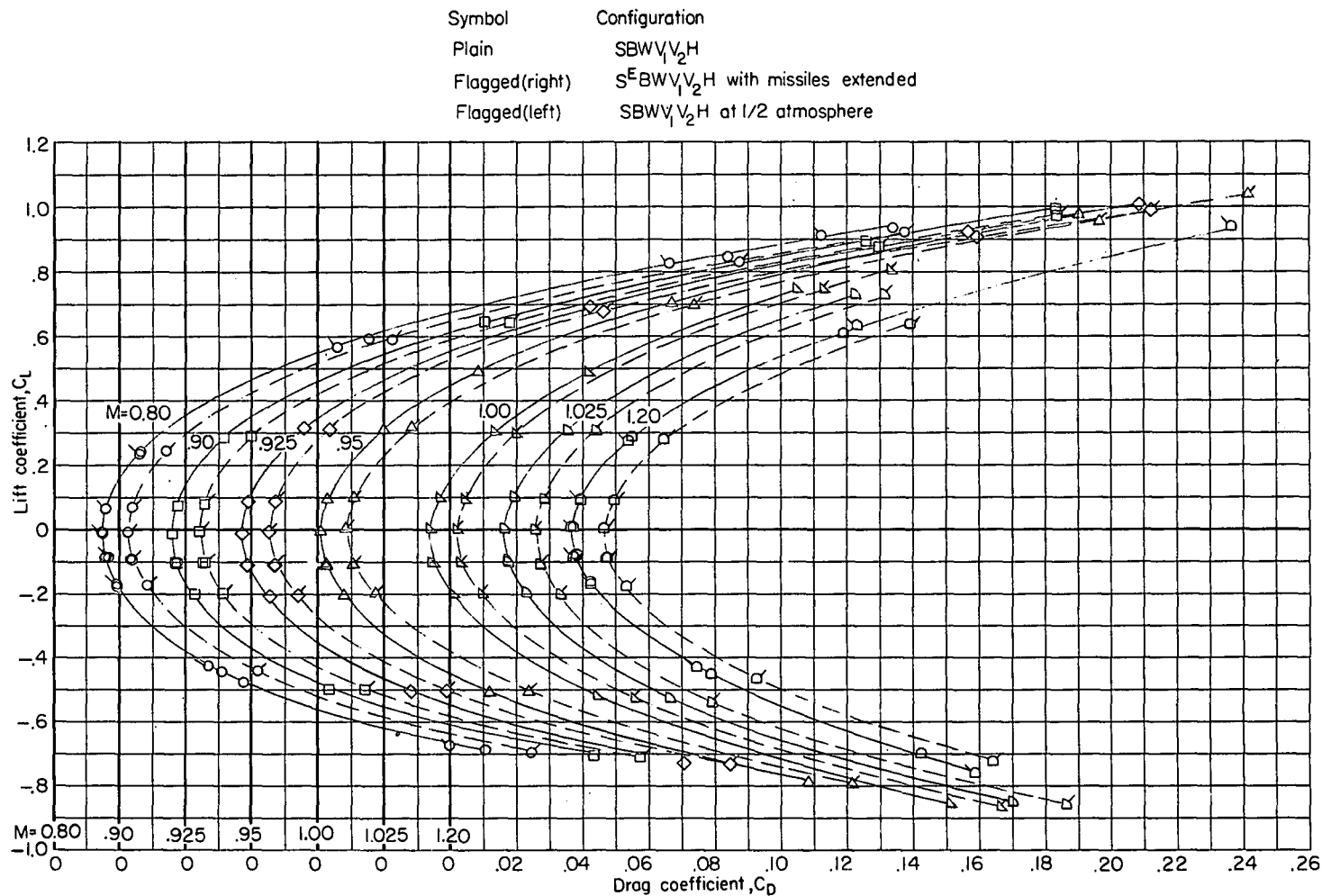
Figure 11.- Concluded.



(a) Angle of attack.

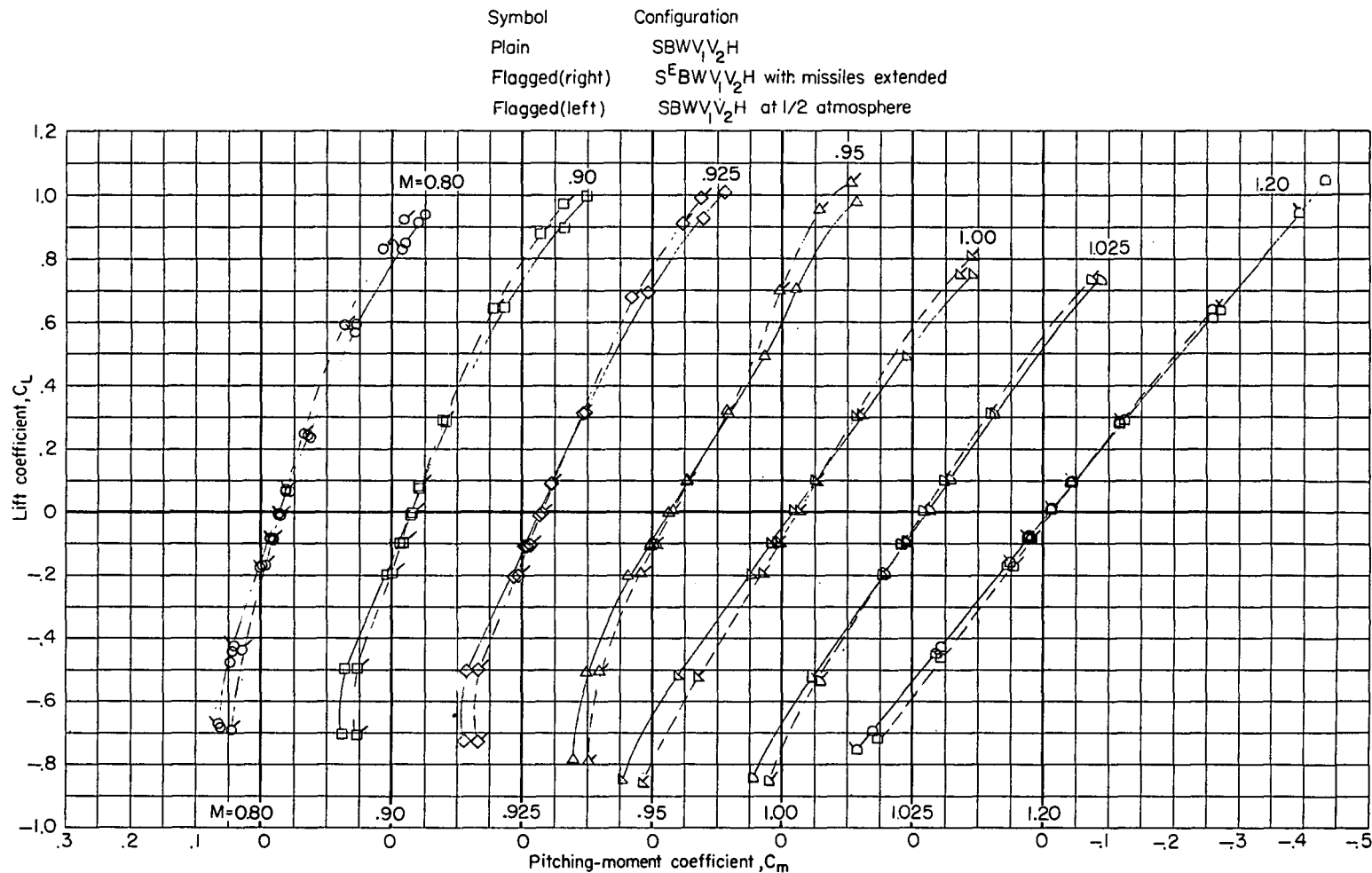
Figure 12.- Effect on longitudinal-stability characteristics of missile extension. $i_t = 0^\circ$.

CONFIDENTIAL



(b) Drag coefficient.

Figure 12.- Continued.



(c) Pitching-moment coefficient.

Figure 12.- Concluded.

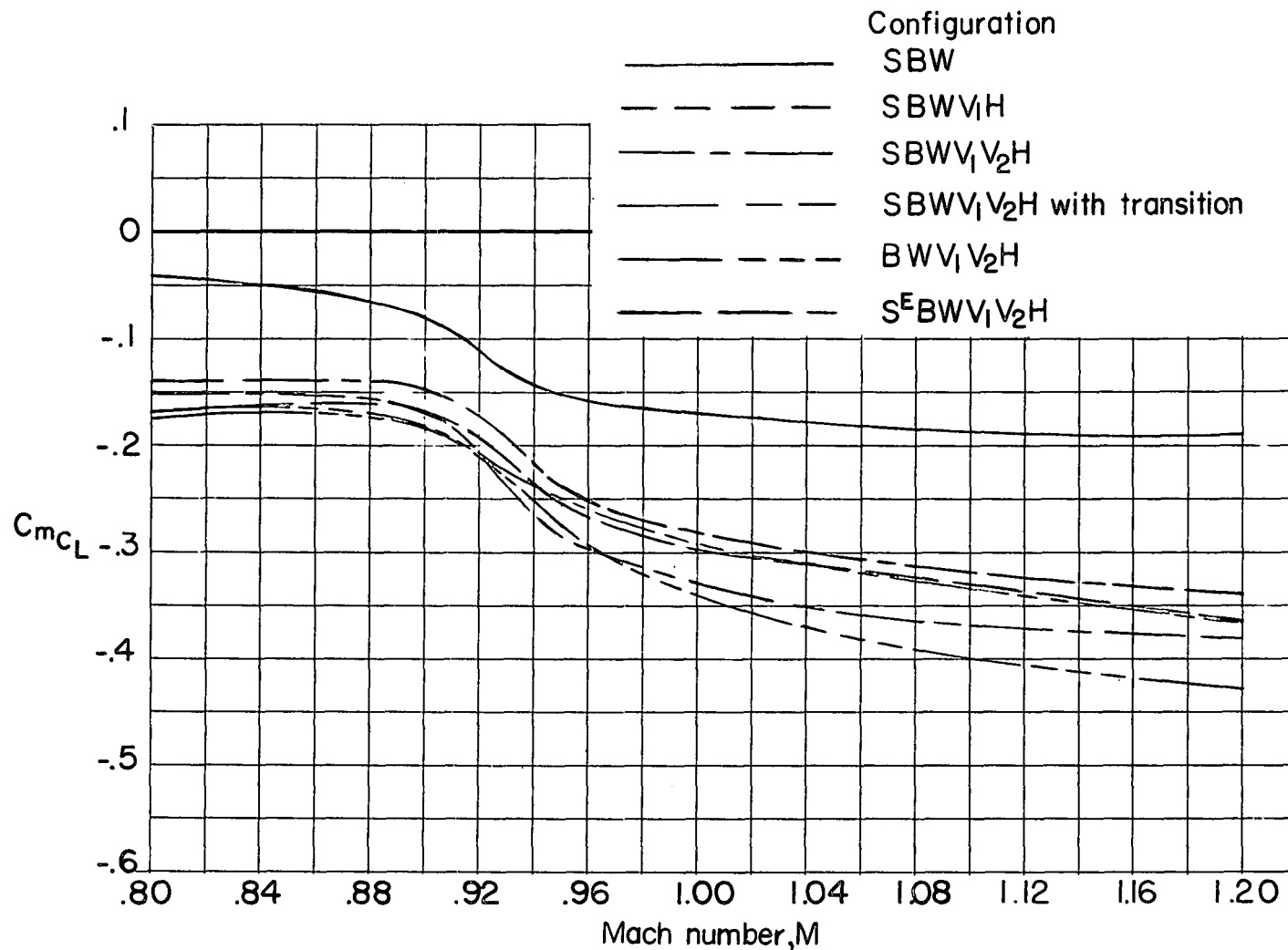


Figure 13.- Effect of Mach number on longitudinal-stability parameter C_{mC_L} . $C_L = 0$.

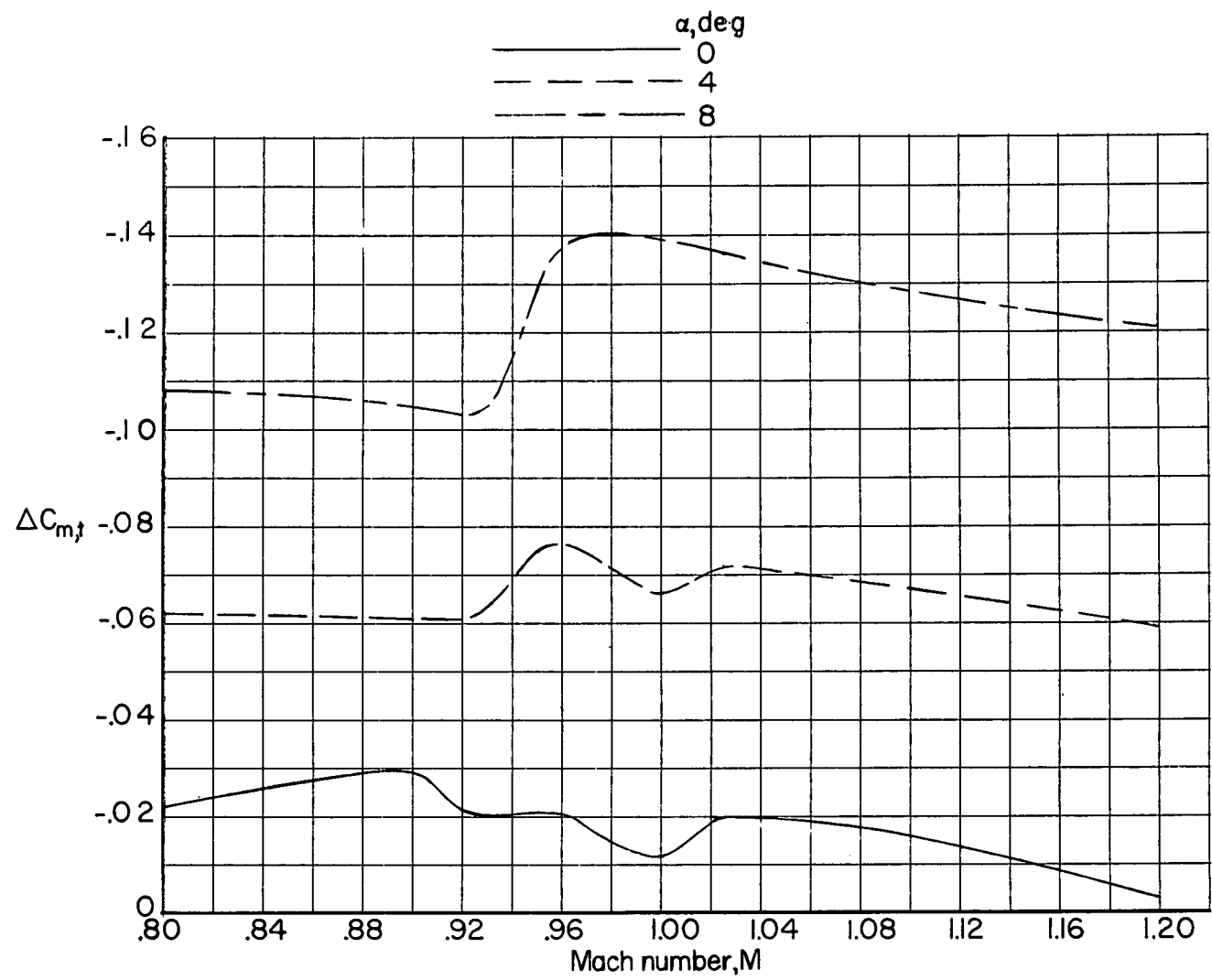


Figure 14.- Effect of Mach number on pitching-moment-coefficient contributions of tail $\Delta C_{m,t}$.

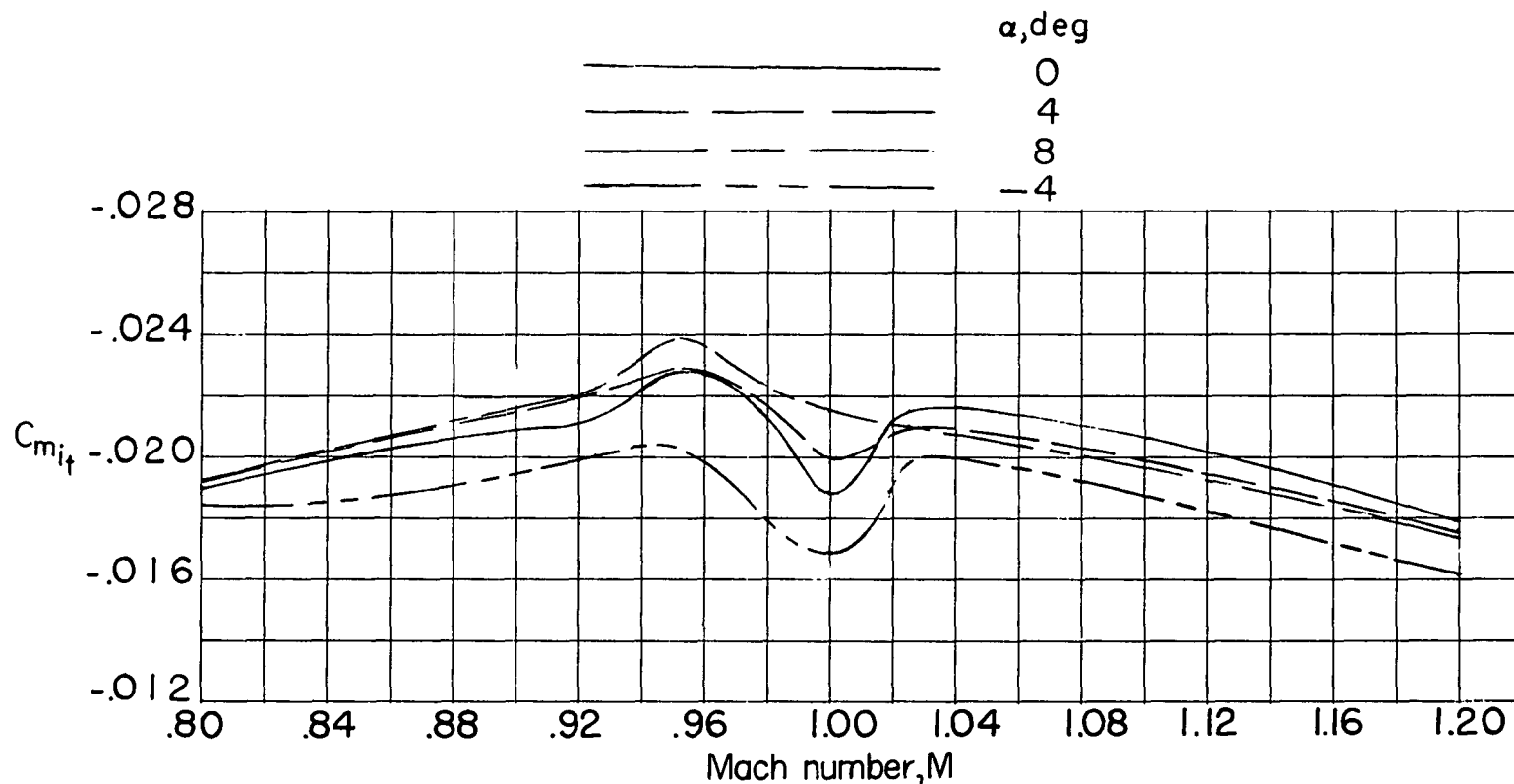


Figure 15.- Variation of stabilizer-effectiveness parameter C_{m1t} with Mach number for several angles of attack.

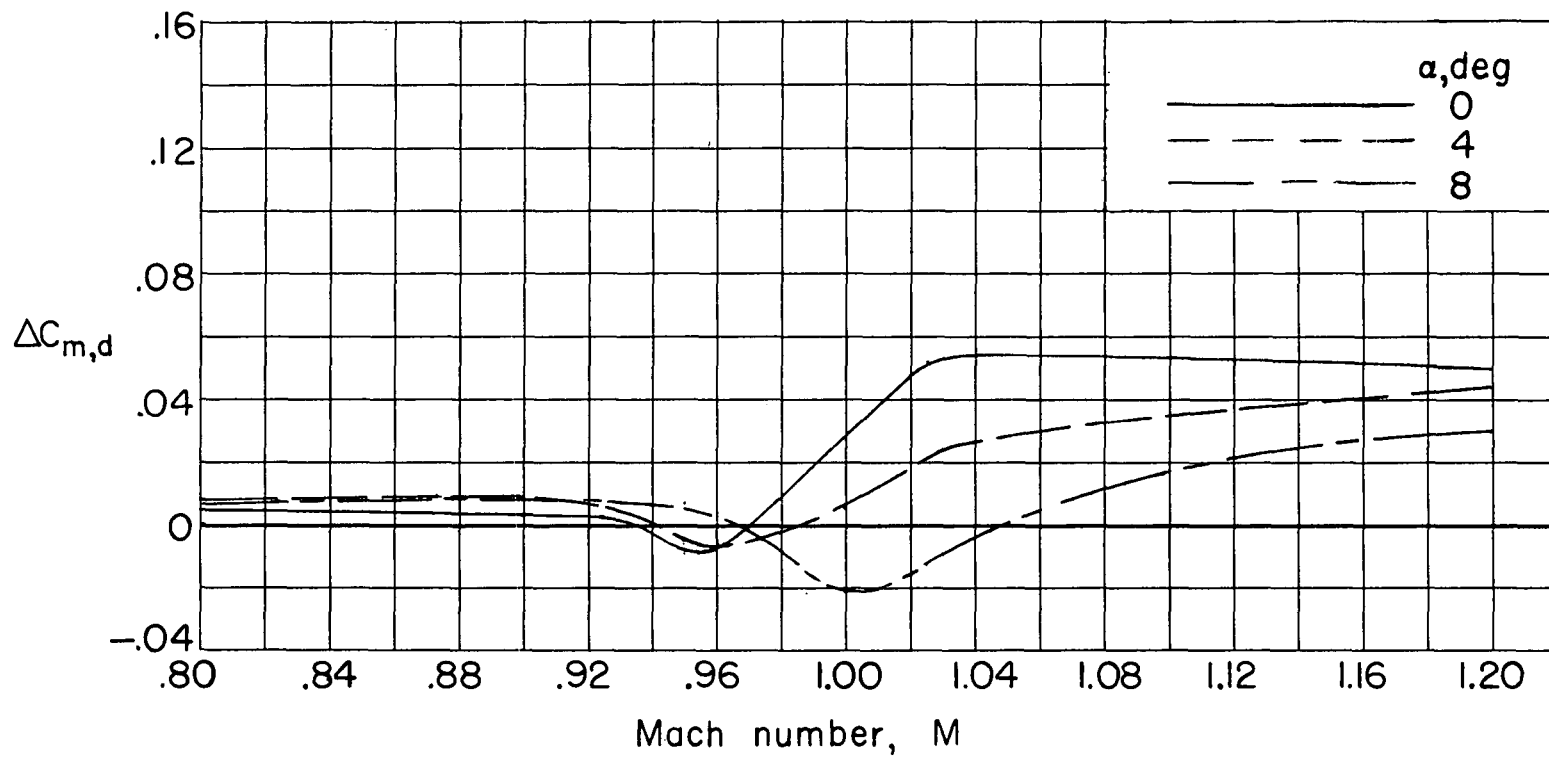


Figure 16.- Effect of Mach number on pitching-moment-coefficient increment due to speed-brake deflection $C_{m,d}$.

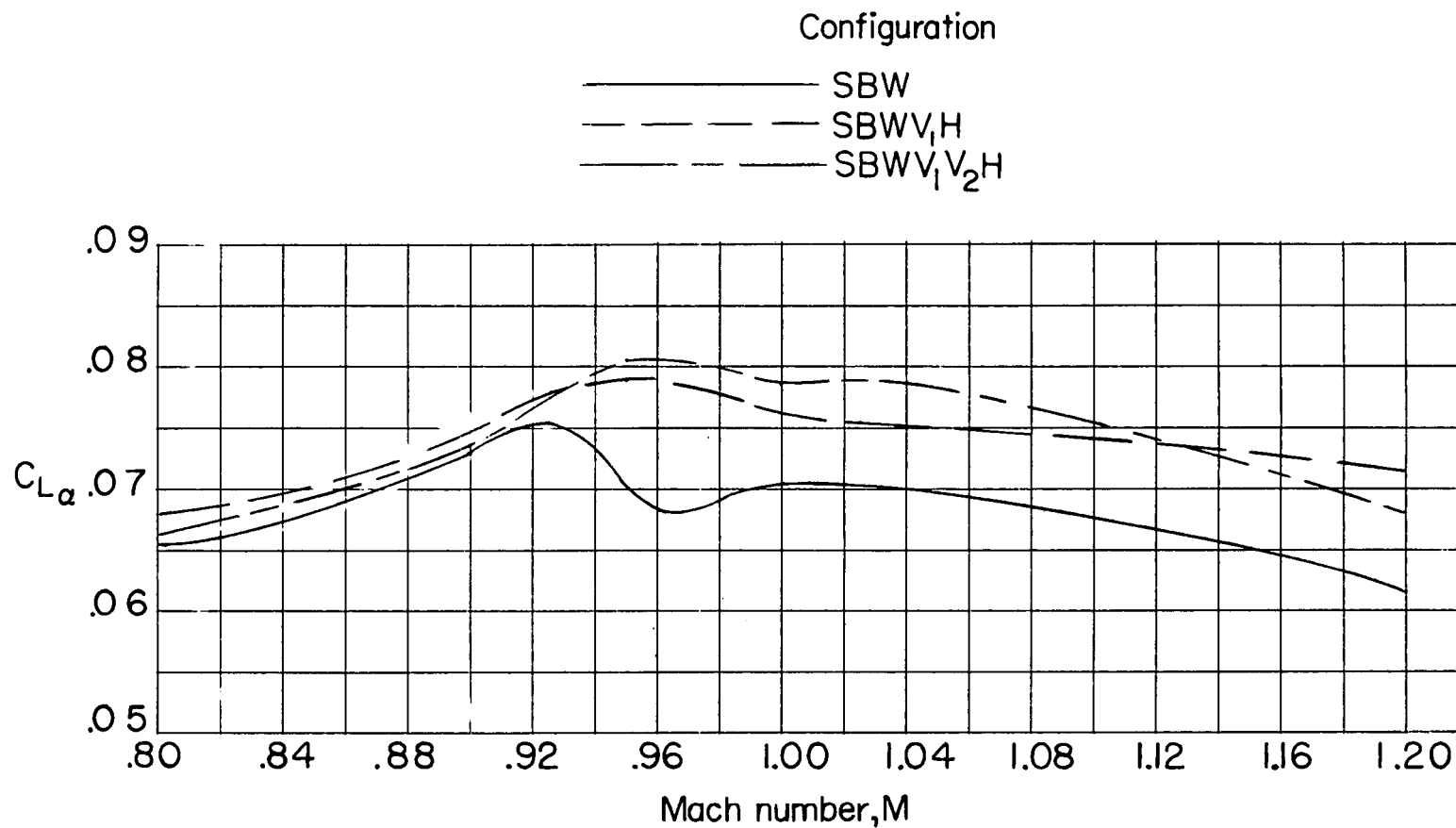


Figure 17.- Effect of Mach number on lift-curve slope. $C_L = 0$.

CONFIDENTIAL

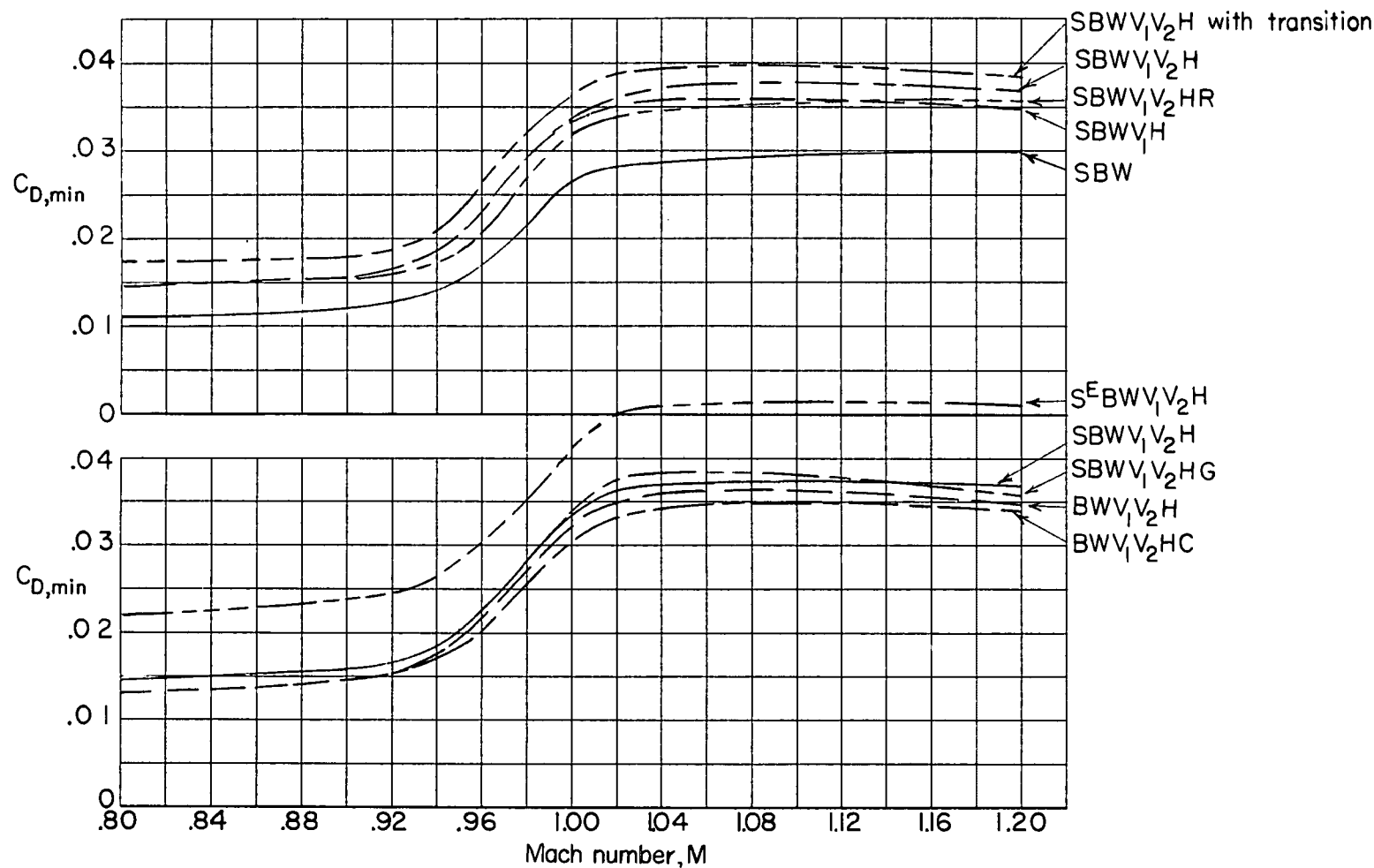


Figure 18.- Effects of configuration changes on variation of minimum drag coefficient with Mach number.

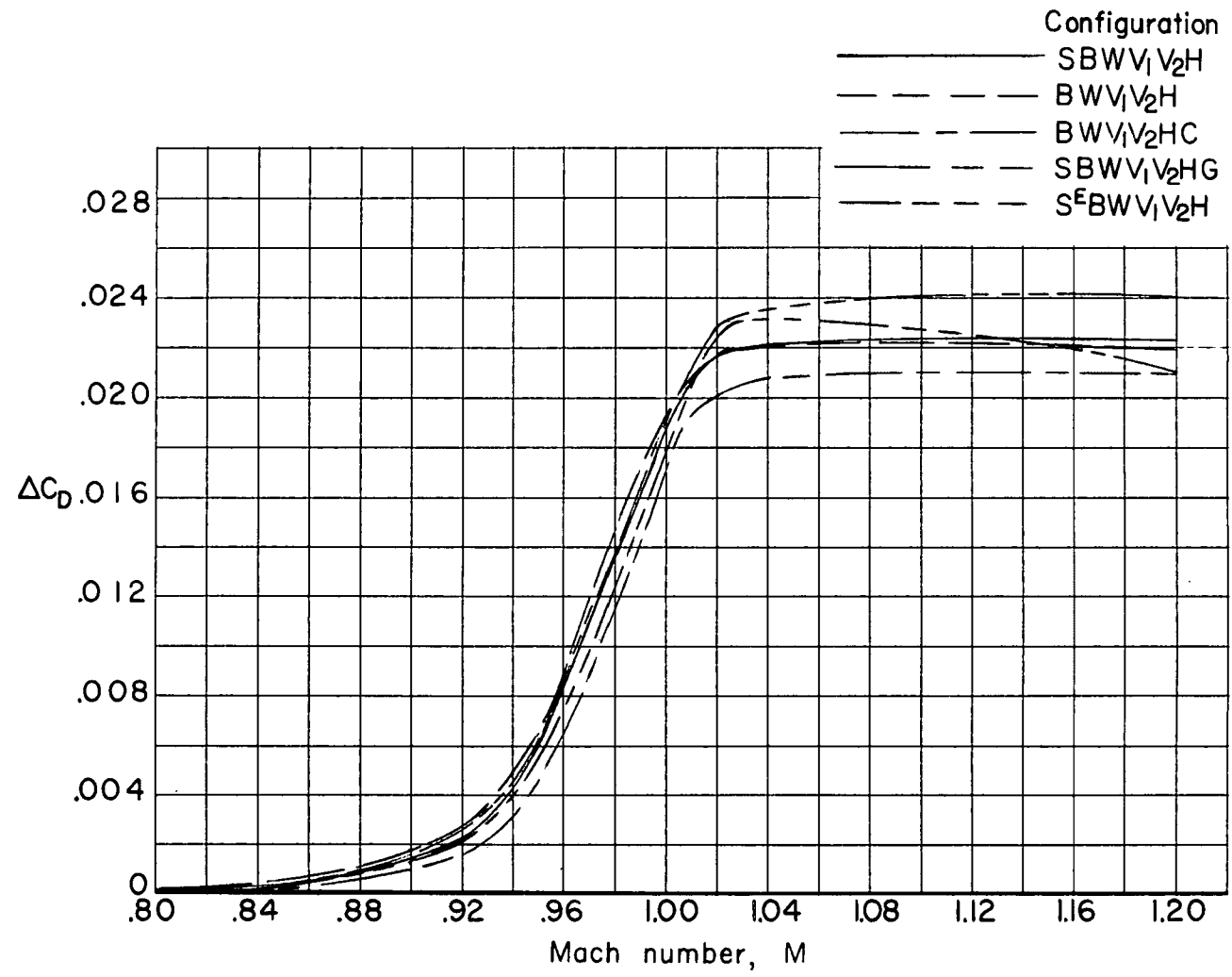


Figure 19.- Effects of configuration changes on variation of drag-coefficient rise with Mach number.

CONFIDENTIAL

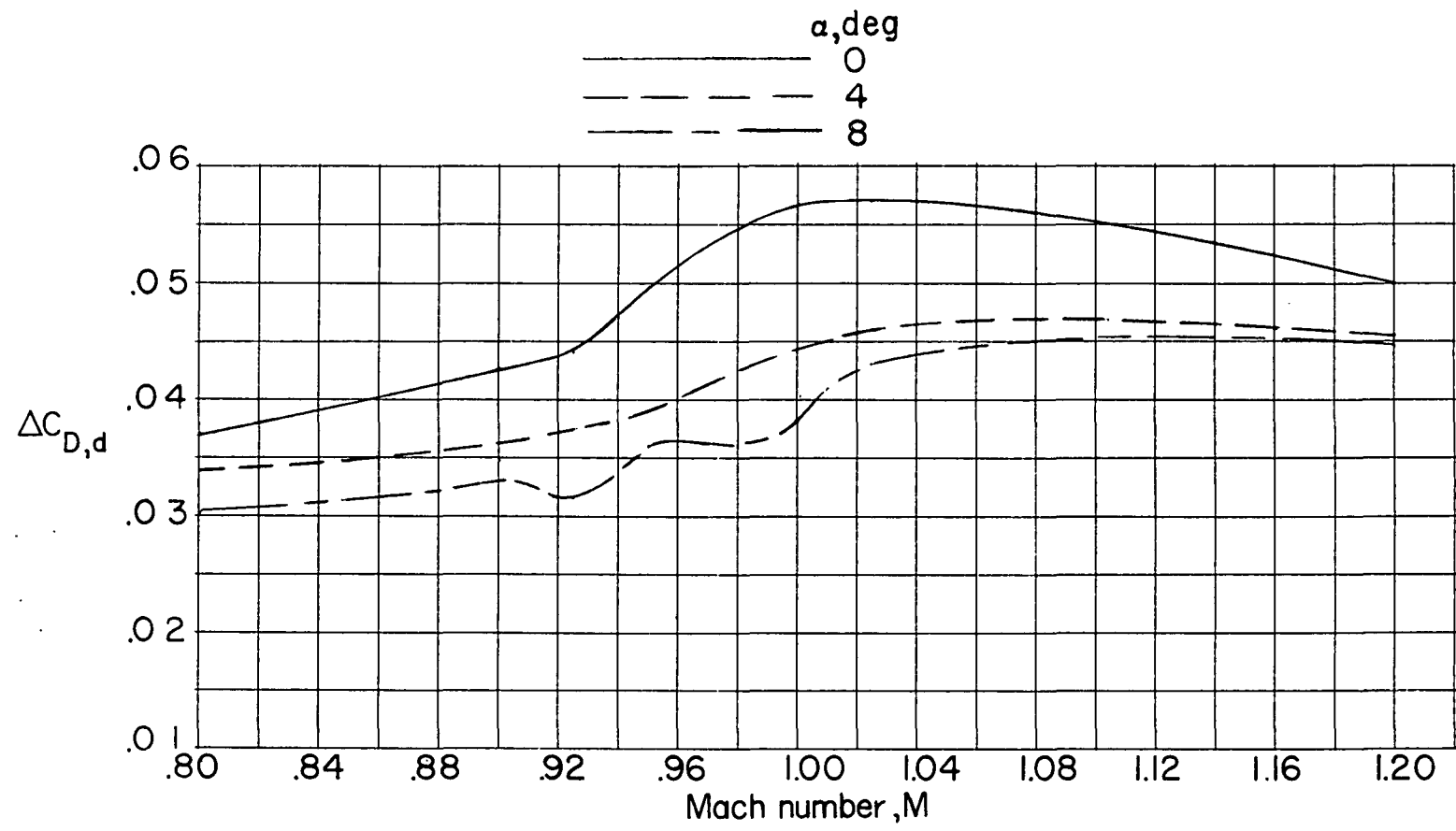


Figure 20.- Effect of Mach number on increment in drag coefficient due to speed-brake deflection $C_{D,d}$.

CONFIDENTIAL

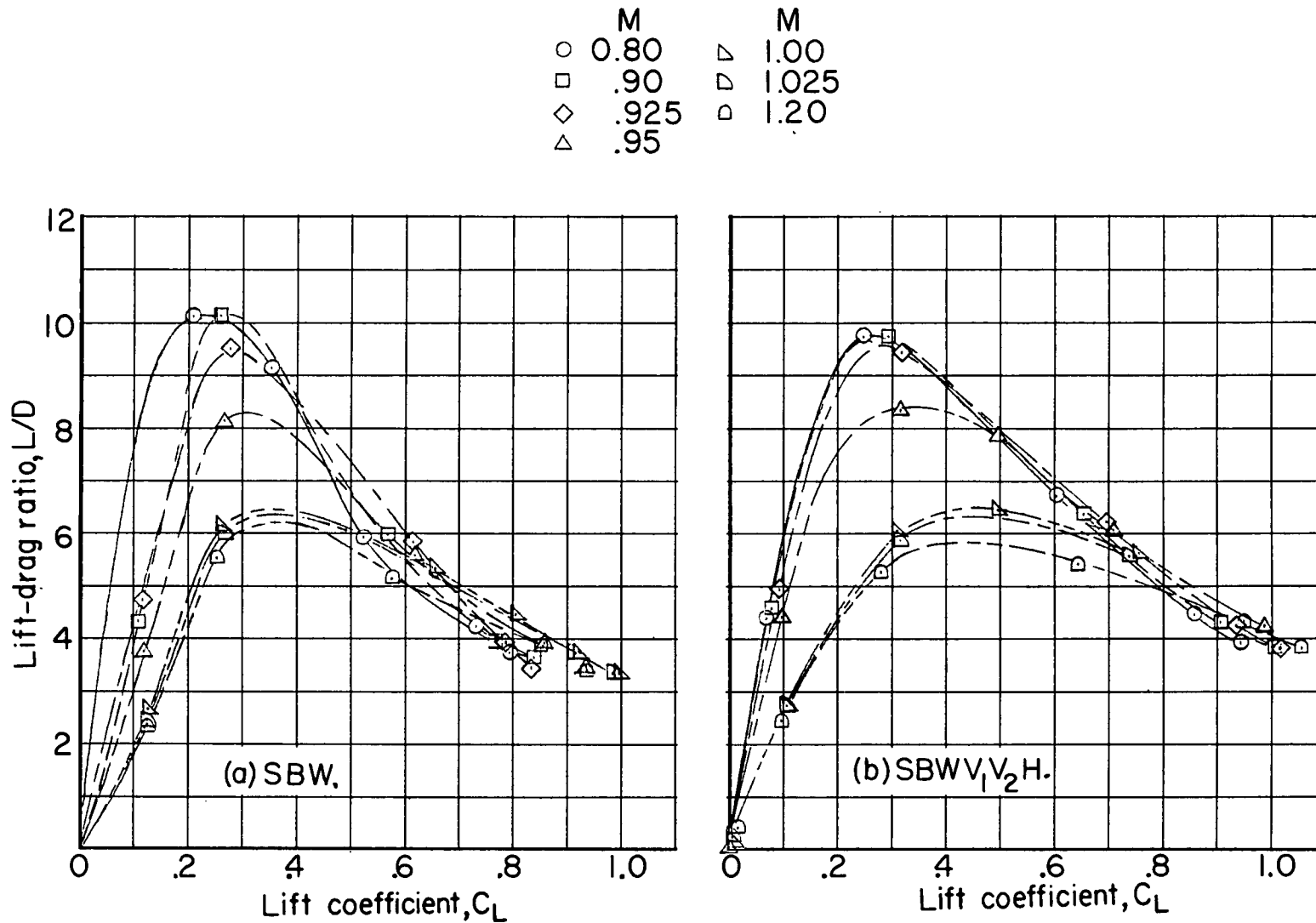


Figure 21.- Comparison of variations of lift-drag ratio with lift coefficient for tail-off (SBW) and tail-on (SBW₁V₂H) configurations.

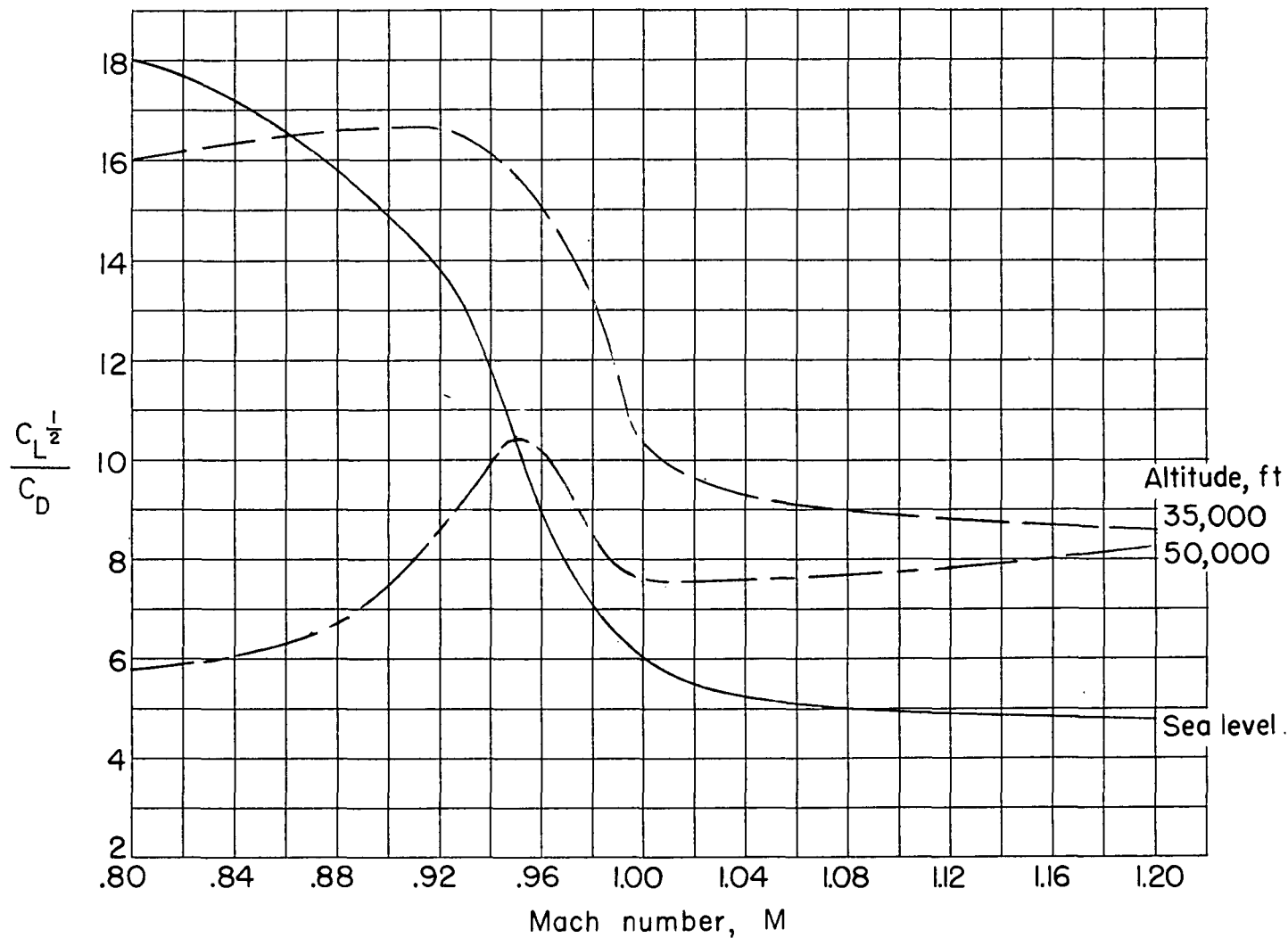


Figure 22.- Variation of range parameter $\frac{C_L^{1/2}}{C_D}$ with Mach number. Combat wing loading.

DECLASSIFIED

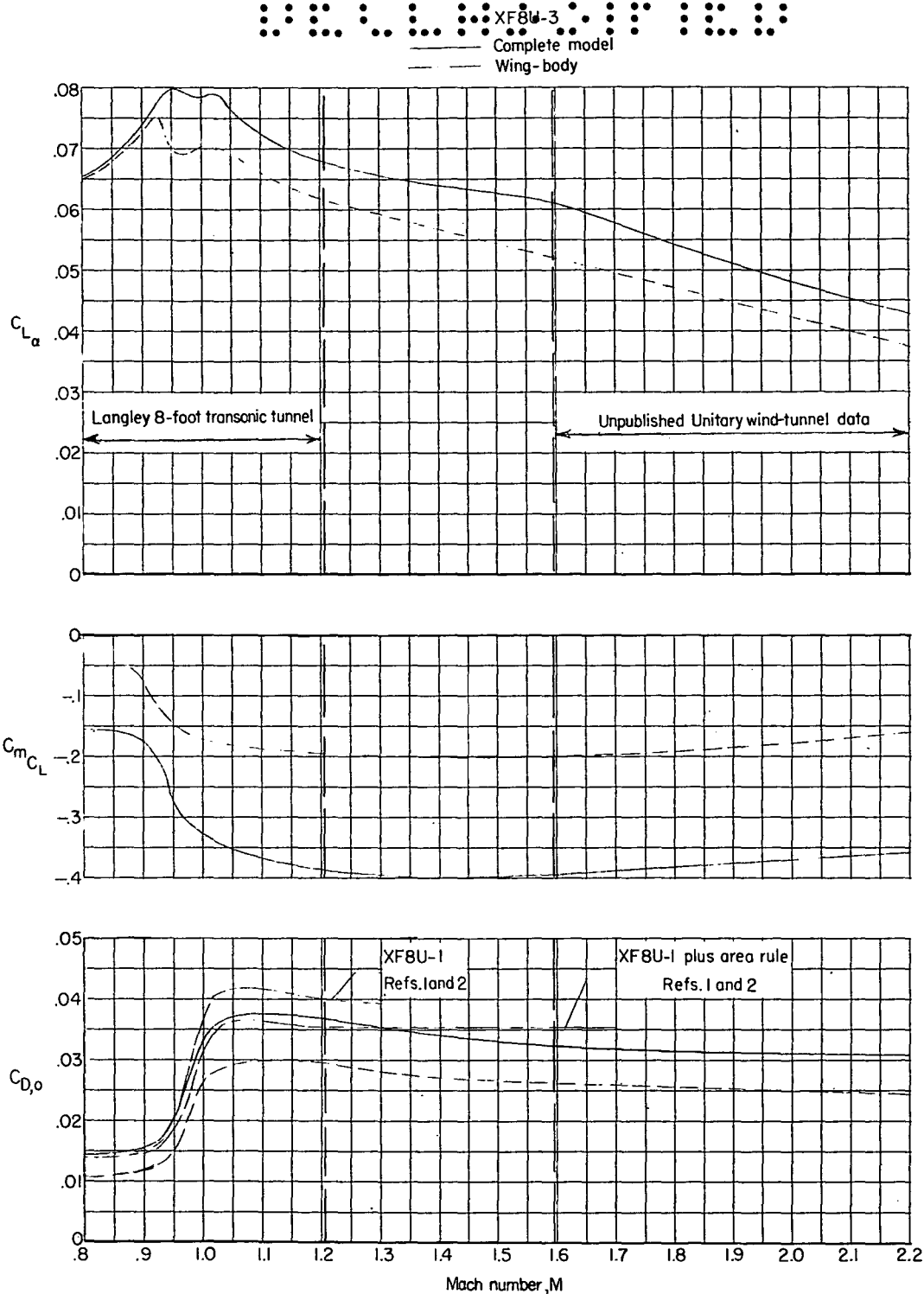


Figure 23.- Comparison of test results at transonic and supersonic speeds.

REF ID: A60180
CONFIDENTIAL

TRANSONIC WIND-TUNNEL INVESTIGATION
OF STATIC LONGITUDINAL STABILITY AND CONTROL
CHARACTERISTICS AND DRAG OF A 0.05-SCALE MODEL
OF THE CHANCE VOUGHT XF8U-3 AIRPLANE

TED NO. NACA AD 3133

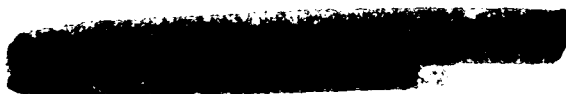
By P. Kenneth Pierpont

ABSTRACT

Investigated were the effects on the model of the addition of ventral fins, speed brakes, missiles, and a fuselage modification. The model was statically stable throughout most of the range of positive lift coefficients, but some loss in horizontal-tail effectiveness may be expected near zero lift and a Mach number of 1.0. Installation of the ventral fins increased the longitudinal stability from 2 to 4 percent at a small drag-coefficient penalty. The speed-brake drag increment decreased with increasing angle of attack, and trim changes of about 2° at low angles of attack may be expected at supersonic speeds.

INDEX HEADINGS

Airplanes - Specific Types	1.7.1.2
Stability, Static	1.8.1.1
Air Brakes	1.8.2.4



CONFIDENTIAL

CONFIDENTIAL